Available online at www.sciencedirect.com

ScienceDirect

journal homepage: www.elsevier.com/locate/he

Review Article

# Alkaline fuel cell technology - A review

*T.B. Ferriday*[*], *Peter Hugh Middleton*

*University of Agder, Department of Engineering Sciences, Norway*

## HIGHLIGHTS

- Alkaline-based discoveries mostly relate to anionic exchange membranes (AEMs).
- Improving the stability of abundant and low-cost catalyst materials is required.
- Notable progress has been made creating AEMs with good stability and conductivity.
- Ionomer-catalyst compatibility is essential during MEA creation.
- A transition from lab-scale to application-level is required to advance AEMs.

## GRAPHICAL ABSTRACT

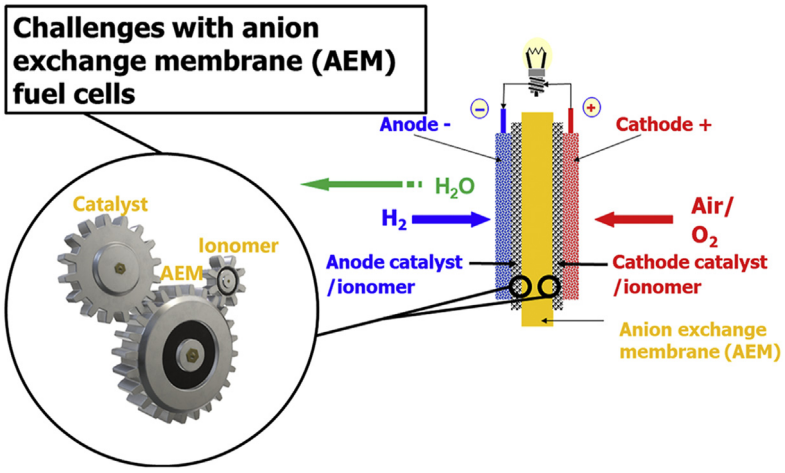


## ARTICLE INFO

*Article history:*
Received 12 January 2021
Received in revised form
24 February 2021
Accepted 25 February 2021
Available online 5 April 2021

*Keywords:*
Anion exchange membrane fuel cell
AEM
AEMFC
AFC
HOR catalyst
ORR catalyst

## ABSTRACT

The realm of alkaline-based fuel cells has with the arrival of anionic exchange membrane fuel cells (AEMFCs) taken a great step to replace traditional liquid electrolyte alkaline fuel cells (AFCs). The following review summarises progress, bottleneck issues and highlights the most recent research trends within the field. The activity of alkaline catalyst materials has greatly advanced, however achieving long-term stability remains a challenge. Great AEMFC performances are reported, though these are generally obtained through the employment of platinum group metals (PGMs), thus emphasising the importance of R&D related to non-PGM materials. Thorough design strategies must be utilised for all components, to avoid a mismatch of electrochemical properties between electrode components. Lastly, AEMFC optimisation challenges on the system-level will also have to be assessed, as few application-size AEMFCs have been built and tested.



* *Corresponding author.*
E-mail address: thomasbf@uia.no (T.B. Ferriday).

https://doi.org/10.1016/j.ijhydene.2021.02.203

## Contents



## Introduction

This review article presents the state-of-the-art in the field of alkaline fuel cells. The main motivation is to provide a single source of information that can be accessed by researches and developers who wish to advance the know-how and create new alkaline fuel cell technologies.

Initially, a brief synopsis of the underlying electrochemistry is given before delving into electrocatalytic materials. The latter will be rigorously reviewed, considering both traditional liquid electrolyte alkaline fuel cells (AFCs) and the more recently polymer anionic exchange membrane fuel cells (AEMFCs) may utilise similar catalyst materials. The AFC description begins with a short historical account of its evolution and elaborates on the materials used, fabrication methods and stacking concepts. The recent trend towards polymer anionic exchange membranes (AEMs) is given thorough coverage as this is deemed the future of alkaline systems. The intrinsic chemistry of the AEM will be briefly detailed in this section, with additional coverage of the most common methods for creating AEMs. AEMFC performances are included and discussed, likewise with ionomer development. Finally, a summary is given where key remaining challenges are outlined, and the road ahead is mapped out.

## Universal components to alkaline-based fuel cells

All fuel cells are based on the principle that fuel reacts at the anode, and air or oxidant at the cathode of an electrochemical system that produces electric power and some excess heat. In this regard, alkaline-based fuel cells are no different from acidic proton exchange membrane fuel cells (PEMFCs). The general workings of an alkaline-based fuel cell, utilising either a liquid or a polymer electrolyte is exhibited in Fig. 1 and the general characteristics in Table 1.

Humidified hydrogen gas is supplied to the anode, which reacts with the hydroxide ions in the electrolyte to produce water and electrons after penetrating the GDL and reaching the catalyst layer (CL), as displayed in Eq. (1)

$$H_2 + 2OH^- \rightarrow 2H_2O + 2e^- \quad E_0 = 0.401\ V_{RHE} \tag{1}$$

A humidified oxygen source, typically purified air/oxygen is supplied to the cathode together with water. Oxygen gas, solvated in water, is reduced at the cathode CL to form hydroxide ions, which diffuse through the electrolyte to participate in the hydrogen oxidation reaction (HOR) that takes place on the anode. The ideal oxygen reduction reaction (ORR) also labelled the direct 4-electron pathway is displayed in Eq. (2).

$$O_2 + 2H_2O + 4e^- \rightarrow 4OH^- \quad E_0 = -0.828\ V_{RHE} \tag{2}$$

Additional highly relevant details to this reaction are further elaborated under the sub-section Oxygen Reduction Reaction. The red-ox reactions in Eqs. (1) and (2) are combined to form the overall mechanism given in Eq. (3).

$$O_2 + 2H_2 \rightarrow 2H_2O \quad E_0 = 1.229 V_{RHE} \tag{3}$$

Equivalently with every other reaction, there are various inefficiencies and losses which lower the achievable potentials in Eqs. (1)–(3). These losses are generally defined as overpotentials and are categorised as charge transfer, ohmic or mass-transport overpotential. These overpotentials variably affect a cell at specific current densities. Charge transfer overpotential is mostly linked with activation losses and is

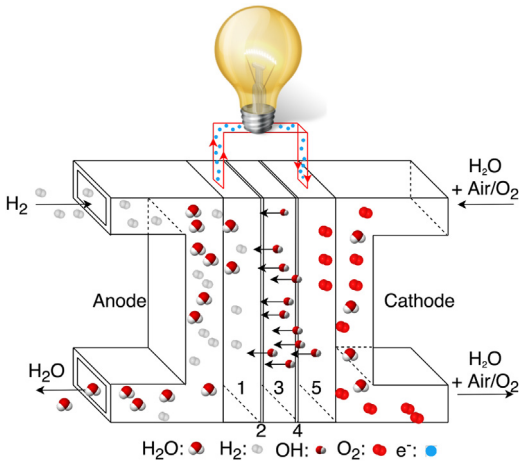


**Fig. 1 – The essentials of alkaline-based fuel cells, where layer 1 and 5 represent the anode/cathode gas diffusion layer (GDL), layer 2 and 4 the anode/cathode catalyst layer (CL) and layer 3 the liquid/polymer electrolyte.**

most visible at low current densities. Ohmic overpotential originates in the electrical resistance of the cell components, determines the slope of the current-voltage graph and is most visible at intermediate current densities. At high current densities the fuel cell will be limited by the speed at which reactants can reach the electrode, inducing mass transportation losses.

Table 1 below displays typical characteristics of both traditional AFCs and contemporary AEMFCs, where record performances and space-related values are included to give a complete view of the two technologies. Comparing the cost of the two technologies is hard, as there is a void in literature on the topic of total AEMFC system costs. One estimation of AEMFC power cost (€ $kW^{-1}$) projected it to lie in the range of ~600 € $kW^{-1}$ (in 2015) [1]. A conservative estimation is that this figure has most likely decreased by a third by 2021, given the increase in AEMFC performance since 2015.

Considering AEMFC technology competes with PEMFCs, complete AEMFC systems must achieve the targeted cost of ~25 € $kW^{-1}$ as set by the US Department of Energy (US DOE) to excel past PEMFCs [2]. Traditional AFC stack system costs were estimated to 100-155 € $kW^{-1}$ in 2005–2007 by AFC Energy and experts in the field (~104–170 € $kW^{-1}$ today) [3,4].

### *Alkaline catalyst materials*

The following sub-section summarises the developments within the various classes of HOR and ORR catalyst materials in an alkaline environment. Focused reviews on this topic may be found in literature for the HOR [14–16] and the ORR [14,17–19].

#### *Hydrogen oxidation reaction*

The hydrogen oxidation reaction and its complement the hydrogen evolution reaction (HER) are two important reactions in several technologies such as fuel cells, chlorine manufacturing and water electrolysis. Comparative to the HOR, the HER has been thoroughly studied through the development of alkaline water electrolysers. There is a notable asymmetry between the anodic (HOR) and cathodic (ORR) fuel cell reactions in terms of applied R&D efforts due to the early focus on surmounting the low exchange current density (ECD) of the ORR ($10^{-4}$ mA $cm^{-2}$ [20] for ORR vs 1 mA $cm^{-2}$ [20,21] for HOR). Consequently, there are many remaining challenges related to developing and understanding electrocatalytic materials for the HOR. There is a large variety of possible fuels for AFC anodes, specifically borohydride, hydrazine, ammonia, methanol, ethanol, and ethylene glycol. The choice of fuel will in turn determine which catalyst materials are available as these depend on the source of hydrogen. The ensuing sub-section pertains only to catalysts developed for the HOR using pure hydrogen gas as fuel.

Studies on HER/HOR have revealed notably slower reaction kinetics in alkaline electrolytes compared to acidic ones, lagging with approximately two magnitudes using the exchange current density (ECD) as a measuring factor [2]. A study on the pH dependence of the HER/HOR affiliated it to a change in the configurational entropy as the proton approaches the electrode surface [22]. Other studies have suggested the hydrogen binding energy (HBE) as a possible sole descriptor of HER/HOR activity [23]. These two theories are joined by a third, that the dissociation of water carries an addition energy barrier which determines the rate of the HER [24]. The exact cause of the poor hydrogen reaction kinetics under alkaline conditions is

**Table 1 – Fundamental features of traditional alkaline fuel cells and the more contemporary anion exchange membrane fuel cells.**

| | AFC [5–10] | AEMFC [5,11–13] |
|---|---|---|
| Electrolyte | 30-40 wt.% KOH | Quaternary ammonia-/piperidinium based polymers |
| Anode catalysts | Pt, Pd, Raney Ni | Pt, Pd, M/N, NiMo, CoNiMo, $Ni_3N$ |
| Cathode catalysts | Pt, Pd, Ag, $MnO_2$ | Pt, PtRu, Pd, Ag, HA[a] –C, $Co_3O_4$, $MnO_2$ |
| Current collector materials | Stainless steel, steel varieties | Stainless steel, steel varieties |
| Temperature (°C) | 40–75 | 50–90 |
| Pressure (bar) | 1–3 | 1–3 (back pressure) |
| Peak Power density (mW $cm^{-2}$) | 50–300 | 100–3500 |
| Current density (mA $cm^{-2}$) | 100–300 | 300–9700 |
| Lifetime (h) | >5000 | 300–5000 |
| Degradation rate ($\mu$V $h^{-1}$) | 3–20 | 7.5–1000 |
| Technology readiness level | Mature | Laboratory Scale |

[a] Refers to hetero-atom (HA) doped carbon materials.

still unknown, and experimental/theoretical findings support all three theories, hence there is uncertainty as to which of the aforementioned theories is closest to describing the cause. The HOR mechanism in alkaline media involves the Tafel and/or Heyrovsky reactions, followed by the Volmer reaction:

$$H_2 \rightarrow H_{ad.} + H_{ad.} \quad (4)$$

$$H_2 + OH^-_{aq.} \rightarrow H_{ad.} + H_2O + e^- \quad (5)$$

$$H_{ad.} + OH^- \rightarrow H_2O + e^- \quad (6)$$

The overall reaction is given in Eq. (1). Either the Tafel or Heyrovsky reaction may be the rate determining step (RDS) at low overpotential depending on the catalyst activity in alkaline media, whereas diffusion of dissolved $H_2$ in the electrolyte has been proposed as the RDS at high overpotential. Many publications specify the Volmer step as rate determining [23,25].

*Platinum groups metals (PGM)*. Platinum (Pt) represents the pinnacle of electrocatalytic performance regardless of whether hydrogen is reduced or oxidised [21]. This has been a favoured material in AFCs as a single, binary, ternary or bimetallic combination similarly with PGMs like palladium, iridium and ruthenium [7]. The acidic ECD of the HOR on platinum lies two orders of magnitude above its alkaline counterpart, in the region of 1 mA $cm^{-2}_{Pt}$ for polycrystalline Pt and carbon-supported Pt [21,26]. The experimental ECD was investigated on commercial Pt/C (46 wt.%) and polycrystalline Pt in alkaline conditions, resulting in values of 0.57 and 0.69 mA $cm^{-2}$ respectively [21].

A breakthrough HOR performance rendering noble-metals obsolete has yet to be displayed, thus many studies have compromised in seeking to instead lower the loading of noble-metals. Hence the effects of Pt/C particle size were investigated [27] and mass activity peaked at 3 nm, though specific activity increased with particle size until levelling off to a plateau value. This increase was correlated with a decline in the ratio of less active edge-atoms [25,27].

Several PtM (M = Fe, Co, Cu, Ru, Au) nanowire alloys performed admirably against the Pt/C (20 wt.%) benchmark e.g. the $Pt_7Ru_3$ yielding an ECD of 0.493 mA $cm^{-2}$, insinuating increased HOR activity from single-dimensional materials [28]. Moreover, a Pt–Ni/C electrode displayed that 3.1 % Pt with 13.9 % Ni resulted in a greater ECD than pure Pt [16,29]. Palladium (Pd) and Pt are similar elements as they both stem from the same group, however Pd is 50x more abundant and paradoxically twice as expensive at the moment [30]. Particle size effects for Pd followed the same trend as Pt [27], the increasing activity levelled off at 19 nm producing an ECD of 0.122 mA $cm^{-2}_{Pd}$ which was attributed an increment of sites with low hydrogen binding energy (HBE).

Pd adlayers were deposited through electroplating $Pd^{2+}$ ions, and through galvanic displacement of underpotential deposited Cu-atoms on a polycrystalline Au substrate [31]. The resulting surfaces comprised 3D Pd structures of unknown depth, where the measure $\theta_{Pd/Au}$ (Pd on Au coverage) varied inversely with HOR activity in 0.1 M NaOH. The ECD varied from 0.022 to 0.003 mA $cm^{-2}_{Pd}$ from low to high Pd coverage. Encouraging results have been achieved with Pd–$CeO_2$/C anodes, where mass specific ECDs of 20 A $g^{-1}_{Pd}$ and average Tafel slopes of 60 mV $dec^{-1}$ have been reported [32]. The Pd–$CeO_2$ interaction was found to be related to the HOR activity, thus it was optimised resulting in the aforementioned results. Density functional theory (DFT) calculations allude that the interaction between Pd and the oxygen atoms of $CeO_2$ weakens the HBE of the catalyst relative to Pd{111}, implying that the Pd–$CeO_2$ framework weakens hydrogen adsorption, thereby enhancing HOR kinetics.

Despite the considerable price and scarcity of PGMs such as ruthenium and iridium, they are still used in the development of electrocatalytic materials however their employment for AFC applications is increasingly niche compared to the increasing R&D focus on non-PGM catalysts. One example includes work by Wang *et* al. [33] where alloys of iridium, palladium and ruthenium on carbon were found to display greater HOR activity measured against both Ir/C and Pt/C in their pure forms. Namely, the alloys $Ir_9Ru_1$/C and $Ir_3Pd_1Ru_6$/C were found as the most active, exhibiting ECDs of 0.9 and 0.6 mA $cm^{-2}_{cat.}$, compared to Ir/C (0.4 mA $cm^{-2}_{cat.}$) and Pt/C (0.5 mA $cm^{-2}_{cat.}$). The growth in catalytic activity was partly credited a decline in HBE.

*Transitional metals*. Pt is the best electrocatalyst for the HOR, where its performance remains the benchmark against which all non-PGM catalyst materials are compared. Nickel (Ni) based materials have been comprehensively studied as replacements for PGMs due to their high abundance, moderate cost and immunity towards corrosion at high pH. Raney nickel catalysts were an early recipient of attention as a non-PGM HOR catalyst due to its inherent high surface area. The group remains among the most active non-PGM catalysts toward the HOR and was an early non-PGM favourite in AFCs as they could endure the severity of 6.0 M KOH solutions [34,35]. It should be emphasised that it is the high pH of AFC systems that allow metals such as nickel to be considered due to their immunity towards corrosion. Raney nickel is commonly used as support material due to poor HOR activity (ECD ≈ 0.00045 mA $cm^{-2}_{cat.}$) in addition to notable stability-related issues meaning alterations through e.g. doping is necessary [36]. Doping with $Ti_2$ or $Mo_{21.3}$ increased the ECD by a factor of 3.9 and 2 respectively. However this material does not harmonise with contemporary AEMFCs, as the anode exhibits nickel oxide traits (passivation) causing deactivation [37]. Furthermore, it is only functional at high KOH concentrations (≈6.0 M) rendering the comparatively low alkalinities of AEMFCs (≈0.1–1.0 M KOH) insufficient. Additionally, Raney nickel's activation process is not realisable in AEMFCs, as it involves applying a cathodic current to reduce the nickel oxides ($Ni(OH)_2$) which elicits hydrogen evolution thus requiring a bifunctional ORR/OER catalyst [5,37,38].

The activity of nickel nanoparticles on carbon was found to increase significantly upon mildly oxidising the catalyst surface [39]. The transformation from Ni/XC-72 to Ni–NiO/XC-72 results in a specific ECD increasing from 0.0062 to 0.056 mA $cm^{-2}_{cat.}$. The partial oxidation of the catalyst surface results in Ni–NiO/XC-72, where hydrogen is adsorbed onto the nickel surface and the nickel oxide adsorbs hydroxide species.

Usually nickel will strongly adsorb hydrogen resulting in poor HOR activity, however the oxidation process causes an increase of the Gibbs energy of adsorption on the Nickel sites close to surface-NiO, effectively enhancing HOR activity through lowering the overpotential at which the HOR begins.

To increase the HOR activity and stability of nickel, a number of transitional metals (Mo, Co, Fe, Cu) were alloyed through various means creating catalysts such as NiMo [40] and NiCu [41]. Using several in-situ spectroscopic analysis methods, it was determined that the molybdenum did not actively contribute to the HOR, though it affected the electronic structure of nickel by lowering the HBE to more thermoneutral values thereby increasing the alloy's HOR activity [40]. The NiMo on Ketjenblack (KB) produced a ECD of 0.027 mA $cm^{-2}_{cat.}$ (4.5 A $g^{-1}_{cat}$) which is highly competitive with other nickel-based electrodes. Furthermore, the resulting MEA remained stable for ≈ 100 h, however significant degradation was displayed between 100 and 115 h.

An array of NiCu alloy films were created by employing a magnetron cosputtering method, where the films exhibited a volcano-like dependence on the increasing atomic fraction of copper [41]. The ECD peaked at 40 at.% copper producing 0.034 mA $cm^{-2}_{cat.}$ and increased the material's resistance to oxidation. The role of transition metals (TMs) in binary Ni-TM alloys was investigated where the authors suggested that the binding energy of both hydrogen and hydroxide should be collectively considered as descriptors of HOR activity [42].

Moreover, an excellent $Ni_3Fe_1$/C catalyst material was created resulting in an ECD of 0.060 mA $cm^{-2}_{Ni}g^{-1}_{Ni}$, (0.96 A $g^{-1}_{Ni}$, low due to the considerable concentration of catalytically inert TMs). Employing a chemical reduction synthesis method might be beneficial for creating efficient HOR electrocatalysts compared against e.g. a thermal reduction synthesis method resulting in the NiMo/KB electrode [40].

The stability of several binary $Ni_3$TM (TM = Mo, Fe, Co, Cu) alloys was investigated, where all except $Ni_3$Mo retained initial activity following 1000 cycles (≈720 h between 0 and 0.3 $V_{RHE}$), however extending the range to 0.7 $V_{RHE}$ caused the formation of $Ni(OH)_2$ through dissolution precipitation for all cases [43].

Ternary nickel alloys have also been explored as HOR electrocatalyst materials, where a CoNiMo electrode displayed an excellent HOR activity when electroplated onto a gold disk [44]. The ternary material outperformed electroplated NiMo and pure Ni, and was responsive to the ratio of its components. The ideal ratio determined was 0.12:5.10:1.00, resulting in an activity 20x that of Ni and was expected to surpass that of Pt. While the catalyst displayed a noteworthy improvement over pure Ni, it still failed to match the Pt benchmark when measuring the ECD (0.015 mA $cm^{-2}_{cat.}$ vs 0.610 mA $cm^{-2}_{cat.}$ for Pt).

The employment of heteroatoms such as nitrogen and boron as dopants in TM-based catalysts is an established practice in the development of alkaline ORR catalyst materials, and this trend has spread to HOR catalyst development. By utilising heteroatoms as dopants, the electronic structure of the TMs changes, thereby altering the HBE and increasing HOR activity. A $Ni_3N$/C catalyst was developed using a hydrothermal method resulting in a specific ECD of 0.014 and 0.017 mA $cm^{-2}_{cat.}$ for carbon-supported and unsupported $Ni_3N$ respectively [45]. Moreover, the supported catalyst yielded remarkable mass normalised activity of 12 A $g^{-2}_{cat.}$. Investigations using spectroscopic techniques revealed a decrease in d-band energy when comparing Ni to $Ni_3N$. Interfacial charge transfers between $Ni_3N$ and the carbon support and a decline in d-band energy resulted in a likewise lowering of the binding energies of oxygen species and hydrogen thus improving HOR activity. The ECD retained 59.8% of its original value after 5000 cyclic voltammetry (CV) scans, thereby displaying the stability of the $Ni_3N$/C catalyst.

A similar nitrogen-doped TM catalyst was created through cathodic electrodeposition followed by thermal nitridation producing a $Ni_3N$/Ni/NF (NF = nickel foam) catalyst [46]. The performance of the $Ni_3N$/Ni/NF surpassed that of Pt/Ni and Ni/NF by 1.4x and 17.6x respectively as shown in Fig. 2a, producing an ECD of 3.08 mA $cm^{-2}_{geo.}$ (calculated from the geometric area of the electrode) or 0.003 mA $cm^{-2}_{cat.}$.

The catalyst was efficient for both hydrogen evolution and oxidation, surpassing many established PGM and non-PGM HER catalyst materials as seen in Tab. S3 in Ref. [46]. The geometric and electronic build of $Ni_3N$/Ni resulted in an intersection between $Ni_3N$ and Ni which yielded excellent sites for hydrogen adsorption with free energy changes close to zero according to DFT calculations. The stability and CO-tolerance was tested, and the $Ni_3N$/Ni/NF exhibited agreeable results compared to the Pt/NF benchmark, as displayed in Fig. 2b-d.

While the aforementioned efforts applied the nitrogen dopant on the catalyst itself, a different group elected to modify the carbon support [47]. The electrocatalytic performance of Ni nanoparticles was increased by the N-doped

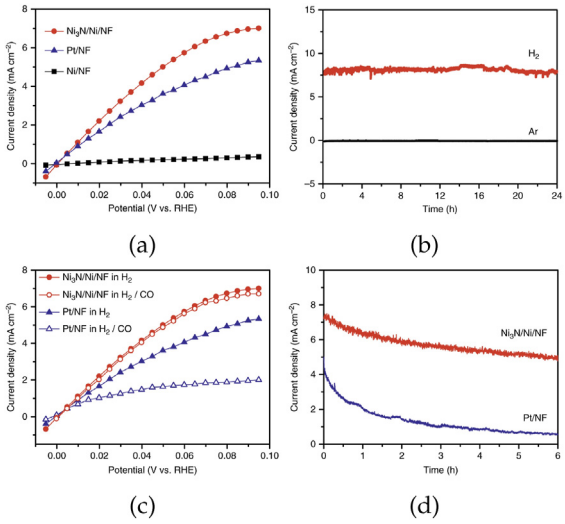


**Fig. 2 – (a) Steady-state polarisation curves of $Ni_3N$/Ni/NF, Ni/NF, and Pt/NF in $H_2$-saturated 0.1 M KOH [46]. (b) Chronoamperometry (CA) of $Ni_3N$/Ni/NF in Ar- and $H_2$-saturated 0.1 M KOH at 0.09 $V_{RHE}$ [46]. (c) HOR polarisation curves for $Ni_3N$/Ni/NF and Pt/NF in 0.1 M KOH saturated with $H_2$ or $H_2$ w/2 vol.% CO [46]. (d) CA comparing CO tolerance of $Ni_3N$/Ni/NF and Pt/NF in 0.1 M KOH saturated in $H_2$ w/2 vol.% CO at 0.09 $V_{RHE}$ [46]. No iR-compensation was employed.**

carbon nanotube (CNT) support by 21x (ECD) and 33x (mass activity). The increase of ECD and a mass activity to yield 0.028 mA $cm^{-2}_{cat.}$ and 3.5 A $g^{-1}_{cat.}$ was explained by DFT calculations. The nitrogen-dopant (specifically the edge-placed N atoms) affected the d-band structure of Ni, resulting in lower HBEs and the support material stabilised the Ni nanoparticles against reconstruction.

Similar results were reported in a more recent study, for an array of Ni catalysts with carbon supports doped with either sulphur, boron or nitrogen created through a two-step pyrolysis and reduction method [15].

The three catalysts all showed an increase in electrochemical surface area (ECSA) compared to the pure Ni/C as seen in Fig. 3. The specific activity (ECD normalised for catalyst loading) follows the sequence Ni/S–C > Ni/N–C > Ni/C > Ni/B–C. The Ni/S–C displayed an ECD of 0.0402 mA $cm^{-2}_{cat.}$ and mass activity of 7.44 A $g^{-1}_{cat.}$, surpassing the N-doped Ni which yielded an ECD and mass activity of 0.0299 mA $cm^{-2}_{cat.}$ and 4.82 A $g^{-1}_{cat.}$. The augmented ECSA was associated with the dopants enhancing the production of small uniform particles due to an anchoring effect, resulting in additional nucleation sites and higher nucleation rates. The increased specific activity was affiliated with the interaction between the catalyst and the support lowering the HBE.

To provide perspective, the specific exchange current densities of all HOR catalyst materials hitherto mentioned in this review are summarised in Table 2. Further figures displaying HOR catalyst performances may be found in the following review papers [14–16,48].

*Oxygen reduction reaction*

The cathodic oxygen reduction reaction (ORR) has occupied the limelight in terms of fuel cell catalyst development ever since the inauguration of the fuel cell. This is due to the large possible overpotential associated with the laborious transfer of four electrons in addition to several possible intermediates.

The ideal ORR displayed in Eq. (2) is also named the direct 4-electron pathway, as it constitutes one of two possible ways this reaction may proceed by (as is commonly accepted). The ORR is a complicated process involving intermediates and the transfer of four coupled proton and electron steps, which leads to several viable reaction pathways. There is still uncertainty surrounding the exact progression of the mechanism, and its complete characterisation is viewed as one of the leading challenges of its field. Due to the high pH in alkaline ORR, superoxide and peroxide ions take part in the other reaction, the alternative "2 + 2 electron" pathway displayed in Eqs. (7) and (8).

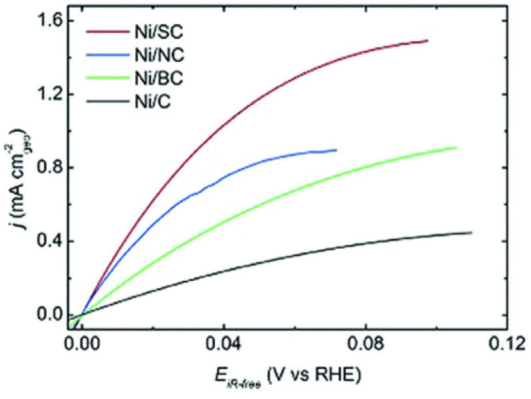


**Fig. 3 – HOR polarisation curves of Ni/SC, Ni/NC, Ni/BC, and Ni/C in hydrogen-saturated 0.1 M KOH (scan rate of 5 mV $s^{-1}$ at 2500 rpm) [15]. Reproduced from Ref. [15] with permission from The Royal Society of Chemistry.**

**Table 2 – The specific exchange current densities of the various HOR electrocatalyst materials featured in this review.**

| Catalyst material | Specific exchange current density [mA $cm^{-2}_{cat.}$] | Mass activity [A $g^{-1}_{cat.}$] |
|---|---|---|
| Pt | 0.6100 | - [44] |
| Pt/C (commercial) | 1.0000 | 1200 [16,49] |
| Pt/C-TKK | 0.5000 | 60 [27] |
| $Pt_7Ru_3$/C | 0.4930 | - [28] |
| $Pt_7Fe_3$/C | 0.4590 | - [28] |
| $Pd/Au_{PC}$/C (low $\theta_{Pd}$) | 0.0227 | - [31] |
| $Pd/Au_{PC}$/C (high $\theta_{Pd}$) | 0.0032 | - [31] |
| Pd–$CeO_2$/C | 0.0526 | 20 [32] |
| Ru-nanoparticles(3 nm)/C | 0.6300 | 82 [27] |
| $Ir_9Ru$/C | 0.90 | 740 [33] |
| $Ir_3PdRu_6$/C | 0.60 | 728 [33] |
| Raney Ni | 0.00045 | - [36] |
| Raney Ni–$Ti_2$ | 0.00176 | - [36] |
| Raney Ni–$Mo_{21.3}$ | 0.0009 | - [36] |
| Non-activated $Ni_{ED}$/XC-72 | 0.0062 | 5.7 [39] |
| Ch-activated $Ni_{ED}$/XC-72 | 0.0560 | 22.4 [39] |
| NiCu | 0.0340 | - [41] |
| NiMo/KB | 0.0270 | 4.5 [40] |
| CoNiMo | 0.0150 | - [44] |
| $Ni_3N$ | 0.0170 | 1.1 [45] |
| $Ni_3N$/C | 0.0140 | 12 [45] |
| $Ni_3N$/Ni/NF | 0.0030 | 0.048 [46] |
| Ni/N-CNT | 0.0280 | 3.5[47] |
| Ni/CNT | 0.0092 | 0.98 [47] |
| Ni/S–C | 0.0402 | 7.4 [15] |
| Ni/N–C | 0.0299 | 4.8 [15] |
| Ni/C | 0.0138 | 1.0 [15] |
| Ni/B–C | 0.0130 | 2.0 [15] |

$$O_2 + H_2O + 2e^- \rightarrow HO_2^- + OH^- \quad (7)$$

The peroxide ion reacts with the solvent and electrons to form hydroxide ions.

$$HO_2^- + H_2O + 2e^- \rightarrow 3OH^- \quad (8)$$

Another pathway for the produced peroxide includes catalytic decomposition, forming dioxygen and $OH^-$ as shown in Eq. (9).

$$2HO_2^- \rightarrow 2OH^- + O_2 \quad (9)$$

Due to the two possible reaction pathways, emphasis is laid upon creating catalyst materials which promote catalysis through the most efficient way, namely the four-electron pathway.

*Platinum groups metals.* The exchange current density of the ORR on platinum is $10^{-4}$ mA $cm^{-2}$, i.e. two magnitudes below that of the HOR which implies the possibility of a significant

overpotential [14,20]. Platinum is the most efficient catalyst for the ORR with an onset potential of 0.94 $V_{RHE}$, a kinetic current density of 31.5 mA $cm^{-2}$ at 0.8 $V_{RHE}$ [50] and a four-electron reduction of oxygen similarly to all other PGMs. However, at very low Pt/C ratios the overall number of electrons exchanged decreases to approximately two because of the carbon contribution. Keeping the Pt/C ratio equal to 60 wt.% Pt ensures a four-electron reaction [51]. Various techniques have been utilised to reduce the loading due to the high cost of Pt and other PGMs, namely the usage of nanoparticles or alloying PGMs with TMs.

Platinum alloys generally exhibit a higher activity and stability than pure Pt [52,53]. The enhanced electrocatalytic activity of the alloys has been explained by a several theories, specifically a decline in bond distance of Pt–Pt hence promoting the adsorption of oxygen. Additionally, the Pt 5d orbital electron density and the presence of surface oxide layers [51].

Palladium (Pd) is the principle PGM catalyst used to replace Pt used either as an alloy or in its pure form due to their similarity [30]. Pt outperforms Pd in their pure forms, however a Pd-TM alloy reverses this trend [54]. The increased catalytic activity is caused by a decline in the necessary Gibbs free energy affiliated with the electron steps caused by a coupling effect related to the d-orbital between the metals, as Pd and the TM have a low and high d-band occupancy respectively [55]. Similarly with Pt, smaller Pd particle sizes don't always result in increased activity, as the specific activity of 27 nm Pd nanocubes was approximately 4x higher than 3 nm Pd spheres, thereby correlating with earlier reported size-related effects [56,57]. This has been attributed to the active sites being blocked by strong $OH^-$ adsorption on small particles [58]. While Pd might seem an appropriate replacement to Pt, the current associated cost is considerable as the raw cost of Pd greatly exceeds that of Pt.

*Non-PGM noble metals*. Contrary to its rarity, gold (Au) {100} is the most active electrocatalyst towards the alkaline ORR and the low overpotential of 0.34 V in 0.1 M NaOH even beats Pt {110} (0.48 V) in 0.1 M perchloric acid [59,60]. While the four electron pathway was utilised by the {100} Au facet, it only occurred in a tight potential range. Three monofacet crystal Au nanocrystals were synthesised by Lu *et* al. [61] by regulating the form of the particles. It was displayed that clean single-crystalline surfaces could be utilised to produce ORR behaviour similar to bulk gold single-crystal surfaces by employing octahedra and cubes encased with {100} & {110} surfaces. Moreover, the narrow potential range was avoided by using a truncated ditetragonal prism (all sides with {310} facets) which displayed a four-electron charge transfer for the entire investigated range (0–0.9 $V_{RHE}$).

To decrease catalytic expenses, gold alloys have also been explored. Through the chemical reduction of metal salt precursors 1-dodecyne, AgAu alloy nanoparticles were created with average core sizes in the range of 3–5 nm [62]. The optimal performance was measured at 35.5 at.% Au as measured by kinetic current density, number of transferred electrons and onset potential, and was found comparable to the industrial standard Pt/C. The great performance was attributed to an alloying effect causing increased metal-oxygen affinity in addition to the metal-ligand interfacial bonding interactions. Through a simple one-pot hydrothermal method a self-supported AuCuCo catalyst was developed. The bifunctional catalyst displayed a similar electrocatalytic performance to the benchmarks 20 wt.% Pt/C and $IrO_2$, in addition to enhanced stability [63]. This performance was explained by the self-supported 3D-structure, the alloying effect between the three components and rich twin crystals.

Silver (Ag) is another noble metal considered as a potential replacement for Pt because of its high activity towards the ORR and relatively low cost [64]. The ORR can occur with either the "2 + 2", the four-electron process or a mixture, contingent on the electrode potential and the oxidation state of the surface [51]. The ideal weight % of Ag to achieve $n = 3.6–3.8$ (n = number of electrons exchanged) was determined 20 wt.% [65]. Studies on the shape of silver nanoparticles allured that the ORR on silver nanodecahedra contained by the {111}-structure occurred through a direct four electron pathway, contrary to {100}-structure containment [66]. Usage of the {111}-structure resulted in weaker OH-adsorption, yielding more active sites and higher ORR activity.

*Carbon based catalysts*. Non-metal doped carbon catalysts represent a new possibility for replacing PGMs, as these materials have displayed curiously beneficial qualities against the alkaline ORR. Usage of heteroatoms as nitrogen and boron as dopants in support materials such as carbon black or CNTs has produced most agreeable results. This increase in activity has been bestowed onto the charge polarisation elicited by a difference in electronegativity between carbon and dopant, however a complete description has yet to arise [17]. N-doped carbon nanocages displayed satisfactory results with the ORR mainly proceeding via the four electron pathway and had a comparable performance to Pt/C (20 wt.%) in regard to onset and half-wave potential and limiting current density [67]. Moreover, the stability was shown by retaining 88.25% of its activity after 5000 CV cycles. A nitrogen on iron-doped carbon nanofibers and graphene (N/Fe-CG) catalyst was created through electrospinning, resulting in active Fe–$N_4$ sites in the centers [68]. The catalytic activity of the N/Fe-CG catalyst was equivalent to the Pt/C (20 wt.%) benchmark which was outperformed in terms of methanol resistance and stability (in both acidic and alkaline conditions).

N-doped CNTs were utilised as support for a NiCo catalyst where the great activity and stability was accredited a synergistic effect between the active sites of the bimetallic catalyst and the heteroatom-doped carbon support [69]. The stability was determined via chronoamperometry (~28 h at 0.6 $V_{RHE}$) and cyclic voltammetry (5000 cycles between 0.5 and 1.1 $V_{RHE}$), where the NiCo/N-CNT catalyst outperformed the 46 wt.% Pt/C benchmark in retaining 95% of its initial current density compared to the 69% the benchmark managed to withhold.

Porous carbons were decorated with atomically dispersed Fe–$N_x$ species and B-centers (FeBNC) and pyrolysed at various temperatures. The FeBNC-800 catalyst displayed a high activity with a four electron ORR and a high onset potential of 0.968 $V_{RHE}$, comparable to the 20 wt.% Pt/C benchmark (1.012 $V_{RHE}$). Furthermore, the current densities of the two materials at 0.40 $V_{RHE}$ were highly comparable at 5.51 and 5.41 mA $cm^{-2}$ for the FeBNC-800 and 20 wt.% Pt/C respectively. DFT calculations implied that the porous carbon was embellished by the incorporation of the B dopant into Fe–$N_x$ hence lowering the energy

barrier for oxygen reduction and improving the overall performance [70].

Combining a solvothermal method with in-situ doping resulted in sulphur-doped carbon sphere electrodes with a varied atomic % of sulphur [71]. The performance of the material peaked at 4 at.% with a four electron ORR and an onset potential and current density (at 0.5 $V_{RHE}$) of 0.882 $V_{RHE}$ and 5.06 mA $cm^{-2}$. Compared against the 20 wt.% Pt/C benchmark (onset = 0.986 $V_{RHE}$ and 5.87 mA $cm^{-2}$ at 0.5 $V_{RHE}$), the performance was most impressive. The stability of the sulphur-doped carbon sphere electrodes determined by CA (24 h at 0.7 $V_{RHE}$) was superior to the Pt/C benchmark, the former retaining 69% of its current vs. 41% for the Pt/C. Phosphorus was doped into hollow carbon spheres (P-HCP), employing a hydrothermal method where an optimised P-HCP electrode proceeded with a four electron reaction displaying an onset potential of 0.887 $V_{RHE}$ and a current density of 5.4 mA $cm^{-2}$ (at 0.6 $V_{RHE}$). The performance was similar to the 20 wt.% Pt/C benchmark at same loading [72].

*Transitional metal oxides*. Transition metal oxides represent several sub-categories of catalyst materials, where this review includes spinels, perovskites and manganese oxides. Spinels are ternary oxides named after the mineral spinel ($MgAl_2O_4$) with the general structure $AB_2O_4$ which is displayed in Fig. 4. The B-cation is critical as it plays an important role in the activity of the catalyst. The anions of the oxide are organised in an enclosed cubic formation where the A-cation occupies an eighth of the tetrahedral sites, and the B-cation half of the octahedral sites [73–75].

A surprisingly high ORR activity was discovered using $Co_3O_4$ on moderately reduced nitrogen-doped graphene oxide ($Co_3O_4$/N-mrGO) [76]. The $Co_3O_4$/N-mrGO displayed a performance highly comparable to the 20 wt.% Pt/C benchmark, moreover with enhanced stability and durability. An onset potential of 0.930 $V_{RHE}$ and a four electron ORR illustrated the high electrochemical activity of this catalyst.

Perovskite oxides have an $ABO_3$-type crystal structure (see Fig. 4) similar to calcium titanate ($CaTiO_3$) [77], where A is an alkali or more commonly a rare earth metal, and B a transitional metal. The perovskite structure consists of $BO_6$ octahedra (in the center) with cations from A, forming a cubic structure around the center as seen in Fig. 4 [78]. The perovskite structure in Fig. 4 is adaptable and can be subject to considerable lattice mismatch, hence a variety of dopants are eligible on the A and B site [19].

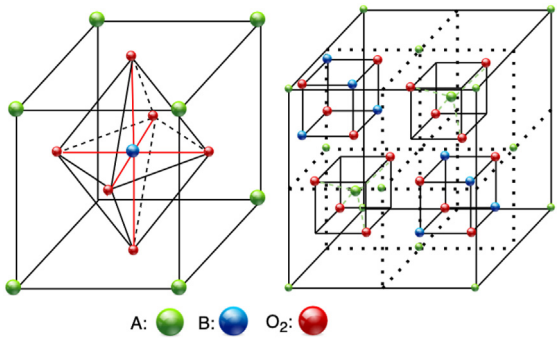


**Fig. 4 – The general structure of perovskite and spinel transition metal oxides respectively.**

Doping $La_{0.8}Sr_{0.2}MnO_{3-\delta}$ with both scandium and phosphorus forming $La_{0.8}Sr_{0.2}MnO_{0.95}Sc_{0.025}P_{0.025}O_{3-\delta}$ resulted in a significant enhancement in onset potential from 0.860 to 0.960 $V_{RHE}$ [79]. Compared against the 20 wt.% Pt/C benchmark, the catalyst displayed a corresponding activity (Fig. 5) and improved stability during a current cycling test.

Manganese oxides have garnered attention due of their low cost, good catalytic activity toward the ORR and abundance, as Mn is the tenth most common element [80]. Various manganese oxide crystallographic structures were investigated, where the activity of $\alpha$-$MnO_2$ was superior to $\beta$, $\delta$ and amorphous structures [81]. The $\alpha$-$MnO_2$ had an onset potential of 0.760 $V_{RHE}$ (compared to 0.860 $V_{RHE}$ for 20 wt.% Pt/C) and increased its stability from 3 to 8 h when doped with Ni. Utilising Koutechy-Levich plots, the electron transfer number of $\alpha$-$MnO_2$ was calculated to 4.2, implying a four electron ORR.

Similarly to the HOR the onset potentials and current densities of all ORR catalyst materials previously mentioned in this review are summarised in Table 3 to provide perspective for ORR. Further figures displaying ORR catalyst performances may be found in the following review papers [14,17–19].

### *Summary*

The focus on developing non-PGM HOR/ORR catalyst materials has increased momentously in the past decade, and accelerated in the period from 2016 to the present with the increase in recorded AEMFC performances. Increased use of in-situ spectroscopic techniques may hold the key to unmasking the particulars of both the HOR and the ORR in regards to intermediates and changes in structure [16]. Insight gained from such advances can hold the key to elevating the performance and longevity of non-PGM catalysts.

## Alkaline fuel cells with a liquid electrolyte

Historically the first real, "useful" fuel cells were based on liquid alkaline electrolytes and metal electrodes using a form

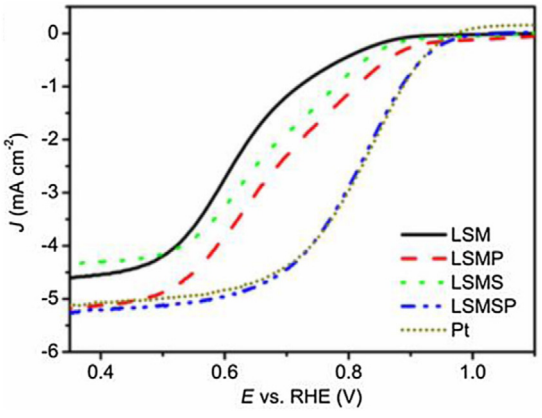


**Fig. 5 – Linear sweep voltammetry curves of $La_{0.8}Sr_{0.2}MnO_{3-\delta}$ (LSM), $La_{0.8}Sr_{0.2}MnO_{0.95}P_{0.05}O_{3-\delta}$ (LSMP), $La_{0.8}Sr_{0.2}MnO_{0.95}Sc_{0.05}O_{3-\delta}$ (LSMS), $La_{0.8}Sr_{0.2}MnO_{0.95}Sc_{0.025}P_{0.025}O_{3-\delta}$ (LSMSP) and Pt/C at 1600 rpm in $O_2$-saturated 0.1 M KOH [79]. Reprinted from Ref. [79] with permission from Elsevier.**

**Table 3 – The onset potentials and current densities of the various ORR electrocatalyst materials featured in this review. The majority of the current densities were measured using a rotating disc electrode (RDE) at 1600 rpm in $O_2$-saturated 0.1 M KOH.**

| Catalyst material | Onset potential [$V_{RHE}$] | Current density [mA $cm^{-2}$] |
|---|---|---|
| rGO-PdPS | 0.940 | 3.20 at 0.4$V_{RHE}$ [50] |
| 40 wt.% Pt/C | 0.940 | 3.25 at 0.4$V_{RHE}$ [50] |
| PdNP/MWCNT(400) | 0.960 | 5.15 at 0.4$V_{RHE}$ [58] (1900 rpm) |
| Au(100) | 0.960 | 2.50 at 0.4$V_{RHE}$ [59] (in 0.1 M NaOH) |
| AuCuCo | 0.946 | 5.65 at 0.4$V_{RHE}$ [63] |
| AuCu | 0.906 | 5.40 at 0.4$V_{RHE}$ [63] |
| 20 wt.% Pt/C | 1.006 | 5.80 at 0.4$V_{RHE}$ [63] |
| Ag-ND/GC | 0.885 | 2.90 at ~ 0.4$V_{RHE}$ [66] |
| C–N-800 | 0.870 | 5.73 at 0.45$V_{RHE}$ [67] |
| N/Fe-CG | 1.040 | 5.05 at 0.4$V_{RHE}$ [68] |
| 20 wt.% Pt/C | 1.030 | 5.10 at 0.4$V_{RHE}$ [68] |
| NiCo/N-CNT | 0.980 | 5.45 at 0.4$V_{RHE}$ [69] |
| 46 wt.% Pt/C | 0.950 | 5.20 at 0.4$V_{RHE}$ [69] |
| FeBNC-800 | 0.968 | 5.51 at 0.4$V_{RHE}$ [70] |
| 20 wt.% Pt/C | 1.012 | 5.41 at 0.4$V_{RHE}$ [70] |
| S–C-2 | 0.882 | 5.06 at 0.5$V_{RHE}$ [71] |
| 20 wt.% Pt/C | 0.986 | 5.87 at 0.5$V_{RHE}$ [71] |
| P-HCP | 0.887 | 5.40 at 0.6$V_{RHE}$ [72] |
| $Co_3O_4$/N-mrGO | 0.930 | 4.52 at 0.4$V_{RHE}$ [76] |
| $La_{0.8}Sr_{0.2}MnO_{0.95}Sc_{0.025}P_{0.025}O_{3-\delta}$ | 0.960 | 5.20 at 0.4$V_{RHE}$ [79] |
| 20 wt.% Pt/C | 0.950 | 5.10 at 0.4$V_{RHE}$ [79] |
| $\alpha$-$MnO_2$-SF | 0.879 | 4.80 at 0.4$V_{RHE}$ [81] |
| $\beta$-$MnO_2$ | 0.859 | 4.15 at 0.4$V_{RHE}$ [81] |

of "zero gap technology" in which the metal electrodes were placed back to back against a thin electrically insulating diaphragm immersed in the liquid electrolyte. The idea of the diaphragm was to prevent the cross-over of hydrogen and air and allow the chemical reactions to take place. In order to supply fuel and air it was necessary to develop a gas permeable electrode that allowed the reactants to reach the active sites of the catalyst but at the same time prevent the flow of liquid electrolyte into the gas channels. This was the birth of the gas diffusion electrode and was a pivotal invention that has subsequently seen many changes over the years. The details of these basic ideas are explained in the following sections.

### *Gas diffusion electrodes*

**The Constitution** of modern AFC gas diffusion electrodes (GDEs) typically include multiple PTFE-bonded carbon black (CB) layers, and the prevailing structure is the double-layer electrode structure shown in Fig. 6, embodying a backing material (BM), a gas diffusion layer (GDL), and a catalyst layer (CL). The location of the BM depends on the design, and can be placed in the GDL, in the CL or in between. A BM requires high gas permeability, structural strength, electronic conductivity and corrosive resistance. AFC current collectors may be composed of e.g. nickel due to its low cost and resistance to corrosion, where meshes or foams are frequently used. Similarly to PEMFC designs, porous carbon paper or carbon cloth may also be utilised [82].

Nickel foam with its substantial pore size and porosity increase liquid/gas flow and extend the electrochemical area, thus enhancing catalyst performance [83]. Furthermore, coating it with various metals has resulted in improved performance. Compared to regular nickel foam, its silver- [84] and gold-plated [85] varieties exhibited lower ohmic and charge transfer resistances.

Reactant gas is supplied to the CL through the GDL, which stops the liquid electrolyte from passing through the electrode. Some leakage is still possible due to the formation of water, an occurrence termed "weeping". The GDL can be fabricated from pure porous PTFE (either PTFE suspension or powder) mixed with ammonium carbonate, where sintering

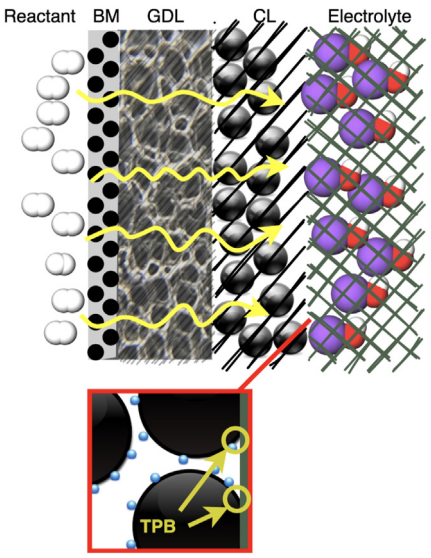


**Fig. 6 – AFC electrode design displayed from the anode side, showing the triple phase boundary (TPB) between electrolyte, catalyst and voids.**

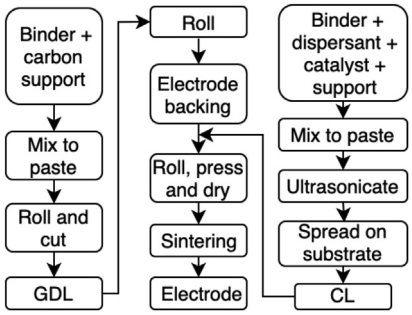


**Fig. 7 – Electrode fabrication procedure.**

(<320 °C) causes gas bubbles to form resulting in a porous PTFE film [10]. Such a GDL has a high electronic resistance, hence should only be used for mono-polar stacks (Fig. 8) such as the Elenco/Zetek designs.

An ideal GDL should be hydrophobic and electronically conductive, where the latter may be achieved by adding CB to the mixture featuring 25–60 vol.% PTFE [86], enabling usage in a bipolar design (Fig. 8). The CL in Fig. 6 comprises the catalyst and its support material bonded with PTFE, where high-surface (500–1000 $m^2\ g^{-1}$) support materials like CB are frequently used to increase power density. Other carbon structures can substitute CB as support to great effect, such as carbon nanotubes (CNTs) [17,47,58], carbon spheres [71,72] and other carbon architectures [67,68]. Stability-issues with carbon supports have birthed a new direction utilising TM-based support-materials for catalysts.

Carbon black is active due its high surface area, a facet which originates in the high temperatures involved in its creation and the pre-treatments specific to each CB type. The surface area of the CB type Ketjenblack was optimised in a $N_2$ atmosphere at 900 °C, while Vulcan XC-72 required $CO_2$ [87]. Complete utilisation of carbon black's high surface area and the affiliated electrochemical activity is coupled to the catalyst's malleability toward uniform distribution over a substrate. Areas not covered are electrically conductive, however they do not participate in the electrochemical reaction. Furthermore the triple phase boundary (TPB, see Fig. 6) between gas, electrolyte and catalyst should cover the entire surface, as catalyst agglomeration causes uneven wear leading to decreased performance and endurance.

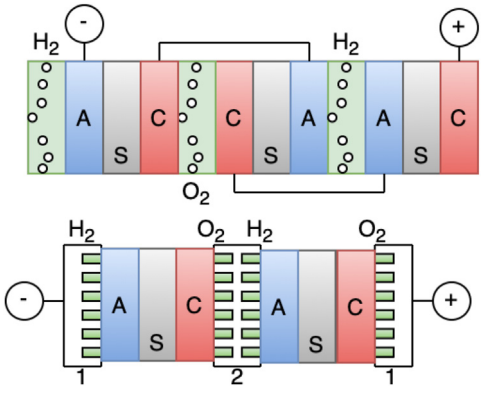


**Fig. 8 – Schematic of mono- and bipolar AFC stacks respectively. A, S and C refer to the anode, separator and cathode. In bipolar stacks, end-plates (1) and bipolar plates (2) ensure electrical conductance between cells.**

The PFTE creates a TPB on the substrate and works primarily as a binder, where the loading (5–25 vol.%) depends on the required hydrophobicity. A metal sheet/grid fixed to the GDL facilitates current collection [88,89]. The traditional design in Fig. 6 has been challenged by integrated anodes, where the GDL and CL were combined through a PTFE-adhered palladium-plated nickel foam [90]. While this design increased the power density, the usage of palladium is questionable. Alternatives to PTFE include the amorphous fluoropolymer material Teflon-AF [91] and Gortex (expanded PTFE) [92] where both have displayed improved AFC performance when measured against PTFE GDEs.

**Fabrication procedures** are highly influential for electrode performance, thus requiring specific emphasis. Displayed in Fig. 7 is a general electrode creation procedure, where many variations exist. Electrode preparation methods are termed either dry or wet methods, pending on whether for instance the binder PFTE is used as a powder or a suspension liquid. The ink-paste method is a common method for creating electrodes, which involves mixing a dispersant and a binder, adding a catalyst powder to create a paste/ink which is subsequently distributed over a substrate either by rolling or screen-printing. Ultrasonication prior to distribution over the substrate ensures a uniform catalyst distribution in the paste/ink, decreases diffusion path lengths and increases the number of gas dissolving sites in the CL.

Recently more advanced methods have been tested, namely electron beam physical vapour deposition which displayed comparable performance to the ink paste method despite a lower catalyst loading, though at an increased cost/difficulty [83].

The process displayed in Fig. 7 is general and variations using filling materials such as ammonium carbonate and added washing/drying stages are hardly uncommon. Development of AEMFC electrodes is an emerging discipline with many approaches derived from traditional AFCs/PEMFCs [13,93].

**Durability** is naturally of paramount importance for an electrode. Anodic degradation rates for an AFC using a Pt/Pd on charcoal GDE were measured to 3.4 $\mu V\ h^{-1}$ after 11,500 h at 100 mA $cm^{-2}$ [7], while the rate for a Raney nickel-based GDE was calculated to 24 $\mu V\ h^{-1}$ after 1500 h [8]. Cathodic degradation rates for an AFC employing Pt-based cathodes have been quantified to 10–30 $\mu V\ h^{-1}$ after 3500 h at 100 mA $cm^{-2}$ [9], 5–10 and 20 $\mu V\ h^{-1}$ at 100 and 200 mA $cm^{-2}$ respectively after 2800 h [10] and 17 $\mu V\ h^{-1}$ for Ag-based GDEs after 3500 h at 150 mA $cm^{-2}$ [94].

There are three principle sources to AFC performance degradation, adsorption of $CO_2$, corrosion and weeping. $CO_2$ is damaging to AFC performance as it reacts with free $OH^-$ ions to form $CO_3^{2-}$ in turn forming a carbonate species (Eq. (10)), exemplifying one of the great downsides to AFCs.

$$CO_3^{-2} + 2K^+ \rightarrow K_2CO_3 \quad (10)$$

Corrosion of carbon materials and deterioration of the hydrophobicity of PTFE due to the electrolyte has been

observed, where $HO_2^-$ radicals from the ORR oxidised the carbon [95]. Carbon-supported catalysts suffer more in alkaline than in acidic electrolytes, where alkaline decline of the ECSA was 3x that of the acidic ECSA after potential cycling between 0.1 and 1.23 $V_{RHE}$ in 0.1 M NaOH [96]. Time-dependant electrode performance reduction is generally caused by an electrode structure flooded with electrolyte, thereby reducing oxygen admittance to the active sites [10]. This anomaly is evidenced by an increased cell capacitance due to a greater part of the electrode is now in contact with the electrolyte. Gortex membranes used in GDEs exhibited increased resistance to flooding compared to commercial GDEs, where 48 h of operation at ~0.858 $V_{RHE}$ (10 mA $cm^{-2}$) in an 6.0 M KOH electrolyte pressurised up to 2.51 bar without leakage provides evidence of this [92].

### Systems

AFC system designs are split between mono- and bipolar systems, where the former was created to simplify the manufacturing process of the GDL as pure PTFE (electrically insulating) could be used. Bipolar designs have the benefit of the interconnection between cells (bipolar plates), which requires an electrically conductive GDL (CB-PTFE composites). Both designs are displayed in Fig. 8.

Monopolar designs benefit from lower costs due to lack of bipolar plates, lower stack thickness due to the singular gas chamber between the electrodes and the ability to disconnect a cell with the remainder of the stack still operating. A significant disadvantage includes a 100 mA $cm^{-2}$ current density limit due to ohmic losses from inefficient current collection [97]. Bipolar designs feature a uniform current density and a higher terminal voltage, rendering it the preferred commercial design [5].

Complete AFC systems are branched into either spacial or terrestrial, the former being pressurised, without cost restraints and impelled by pure $H_2/O_2$, and the latter with low-cost components and powered by $H_2$/air at ambient pressure and low temperature.

### Achievements

**The inauguration** of all AFC systems came through Francis Thomas Bacon, who's cell was built with sintered nickel anodes and lithiated nickel oxide cathodes employing a circulating 30–45 wt.% KOH solution as electrolyte. The 5 kW monopolar system powered by pure $H_2/O_2$ at 200 °C at 45 bars displayed a notable performance [5].

**The 1960s** brought the Gemini space program where a PEMFC was utilised, though the system was found to be inefficient and unreliable due to membrane-related problems. An alkaline system based on Bacon's work was developed to replace the PEMFC for the Apollo missions. Specifications such as the extreme Pt loading of 40 mg $cm^{-2}$, an 85 wt.% KOH concentration and temperatures over 100 °C at 3 bar pressure were applied in 93 cells divided between 3 parallel connected stacks resulting in a 4.5 kW AFC [98].

**In the 1970s** a 7 kW system was developed by Siemens comprising 70 cells driven by pure $H_2/O_2$ operating at 0.4 A $cm^{-2}$ at 0.8 V per cell in 7.0 M KOH at 2 bar, 80 °C. The bipolar system employed a circulating electrolyte and asbestos diaphragms in each electrode to stop gas leakage from the electrolyte side. Development of systems for submarines were the main result of Siemens's R&D efforts [5]. Another company involved in AFC development was the Belgian-Dutch company Elenco, who's R&D efforts resulted in a 200 kW AFC system for a hybrid bus.

**Up to the 2000s**, the UK company Zetek [97] (now Eident Energy) modified a London taxi to be powered by an AFC in 1999 (100 km range), in addition to the first AFC-powered boat in 2000. The majority of commercial interest in AFC development has dried up with some electing to switch to PEMFCs, AEMFCs or producing underlying components such as GDEs, membranes, ionomer, etc. [5].

**Today**, existing companies supplying AFC solutions include the UK-based company AFC Energy and GenCell Energy from Israel. While the former still supplies AFCs at the > 10 kW to > MW scale, the shift towards a solid-state electrolyte (AEMFCs) is pronounced. GenCell announced in 2018 a commercial system including a 4 kW AFC employing cracked ammonia (99.5%) as a hydrogen source (Project Alkammonia) as a stationary off-grid power supply [99]. AFC Energy is a leading partner, as all their standard configurations have the cracked ammonia as a fuel option.

### Summary

The future of AFCs appears to predominantly lie in transferring relevant experiences over to AEMFC technology to accelerate its progress. While there are some companies left that still supply complete AFC systems, the potential for development is deemed greater in PEMFCs and in the near future AEMFCs.

## Anionic exchange membrane fuel cells

Anion exchange membranes (AEMs) are gaining popularity for use in alkaline electrolyser and fuel cell (FC) technologies to replace traditional AFCs. However, there are many challenges to be addressed before AEMs become mainstream, including performance, stability, durability, mechanical strength, and low-cost production methods.

Generally, AEMs offer several advantages over liquid-based alkaline systems, such as better $CO_2$ tolerance, decreased gas crossover, which in the case of electrolysis results in purer hydrogen and for FCs a higher open circuit voltage (OCV) and increased efficiency [12]. Moreover, for FCs the problem of flooding and "weeping" is also largely avoided due to the solid-state electrolyte. One of the greatest AEM challenges is creating a thin membrane (~10 $\mu$m) which can reach a high enough conductivity (>100 mS $cm^{-1}$) to allow it to deliver sufficient current density (>0.5 A $cm^{-2}$) while simultaneously achieving the target of 5000 h of stable operation at 80 °C [12]. Average hydroxide conductivities in AEMs have reached proton conductivities in PEMs [100] (~ 100 mS $cm^{-1}$ at 60 °C [5]), and several exemplary papers report values in the range of 150–300 mS $cm^{-1}$ [100–102].

Similarly to traditional PEMFCs, the conductivity of the membrane is adversely affected by low humidity, due to the

mobility of the $OH^-$-group in the polymer body of the membrane depends on the level of dissociation of the cation–anion groups which require a higher level of solvating water molecules than would be present in the dry membrane. Additionally, AEMs can suffer from embrittlement if stored in dry conditions after activation in 1.0 M KOH. For this reason AEMs are always kept humidified and may be refreshed using a dilute alkali e.g. as 0.1 M KOH, thereby removing any build-up of carbonate species.

Mechanical strength and durability is of great importance as many AEMs are easy to rupture through stresses caused by attaching it to electrode frames and especially in the process of creating MEAs, via the application of catalysts and current collectors. Thus emphasis must be laid upon creating AEMs with a high tensile strength when thin membranes in the range of ~ 10–30 $\mu$m are produced. Such low thicknesses enable AEM fuel cells (AEMFCs) to operate at high peak power densities (PPDs) due to lower mass transport resistance and improved water management [103,104], however this places extensive demands on the mechanical/chemical stability of the AEM [104].

Specifically, hot-pressing methods that are used to make PEM MEAs do not always work optimally with AEMs, hence other bonding methods are needed. Accordingly, some commercially available AEMs are supplied on a backing material providing additional mechanical strength, or supplied with fibre reinforcement for similar reasons.

There are several commercially available AEMs on the market that are being tested and many research groups are developing various improved and advanced AEM systems. Commercial products include: Ionomr (Canada - AFN-HNN8-50-X, AFN-HNN8-25-X, etc.), FuMA-Tech (Germany - FAA, FAB, FAD, etc.) and the US companies Xergy (Xion Durion™, Pention™), Orion (Orion™) and DiOxide Materials (Sustainion®).

Other companies producing AEM-related products include Tianwei (China), MEGA (Czech Republic) and Asahi Chemical Industry Co (Japan) [105–107]. The Pention AEM from Xergy Inc [108,109]. has been employed to produce one of the highest power density associated with commercial AEMs (3370 mW $cm^{-2}$). Many of the commercially available membranes for FC and electrolyser applications have evolved from the chloralkali industry or desalination plants. Presently, the commercial exploitation of AEM technology lies mainly in water electrolysis, where companies such as Enapter already have small kW AEM units. For FCs, the UK company AFC Energy is developing FCs based on AEMs, however their performance data is yet to be published.

### *AEM approaches*

Mainstream experimental AEMs are solid polymer membranes composed of a polymer backbone (f.ex. polyphenylene [110], poly(aryl piperidinium) (PAP) [111–113], polynorbornene [103,108,114], poly(ether-ether ketone) (PEEK) [115], polyethylene [100,116,117], poly(phenylene oxide) (PPO) [118–120], poly(ether sulphone) (PES) [121], polysulphone [122,123]) onto which functional cationic end-groups are attached (f.ex. QA [103,108,114,119], imidazolium [115,120,122,124,125], guanidinium [123] quaternary phosphonium [117,126], cobaltocenium [116], piperidinium [111–113], sulfonium and ruthenium). The

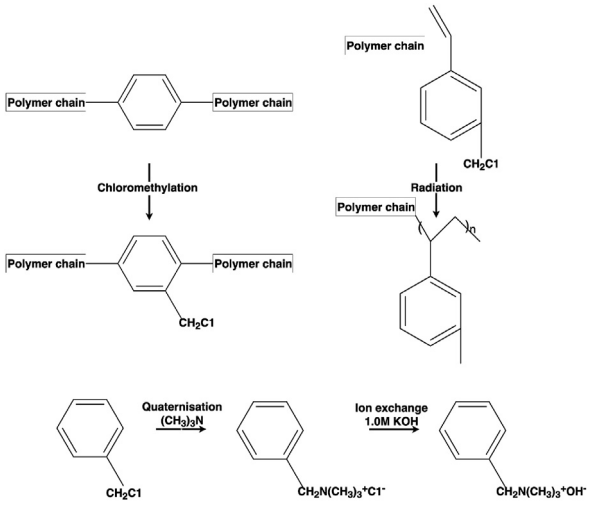


**Fig. 9 – Generic chemical reaction steps to convert a polymer into an AEM with QA as cationic end-group.**

ionic conductivity is assured by mobile $OH^-$-anions associated with the cationic end-groups. Fig. 9 shows the generic chemical reaction steps where a backbone polymer is converted into an AEM polymer with a QA group as the cationic end-group.

There are several possible pathways, where Fig. 9 exhibits two classic examples. First case, the main polymer chain containing a phenyl group such as a polysulphone is functionalised by a chloromethylation reaction. Secondly, a process known as "radiation grafting" is used to attach a vinyl group (vinyl benzyl chloride). The next step for both cases, the QA group is formed by treatment with an amine reagent (quaternisation). Finally, the hydroxide conductivity is induced by treatment with KOH to attach $OH^-$ to the cationic end groups as displayed in Fig. 9.

AEM ionic conductivity depends on the number of functionalised cationic groups, however there is a trade-off with mechanical stability because AEMs tend to swell up in volume as more groups are functionalised. This leads to the main challenge with AEMs – keeping a high anionic conductivity at the same time as high mechanical strength.

Another challenge lies in the paradox that the presence of $OH^-$ in the AEM causes long term degradation, because the $OH^-$ group also acts as a nucleophile that can attack the cation group, thus splitting it into methanol and an amine (Fig. 10a). The effect of nucleophilic degradation has found to be mitigated by placing the cation group at the end of the pendant alkyl chain [127]. A second degradation process is where $OH^-$ attacks via an $\alpha$–$\beta$ Hoffman elimination reaction to form a carbon–carbon double bond and the elimination of water (Fig. 10b).

Fig. 10 displays only a fraction of the various degradation pathways to which AEMs in general are vulnerable, and more extensive accounts may be found in more focused literature [100,104,127–129].

Low-cost polymer backbones available from industry such as PEEK, PPO and polysulphone saw a fair amount of use in the early days of AEM development. However, progress has been made in the chemical stability of AEMs, where issues such as

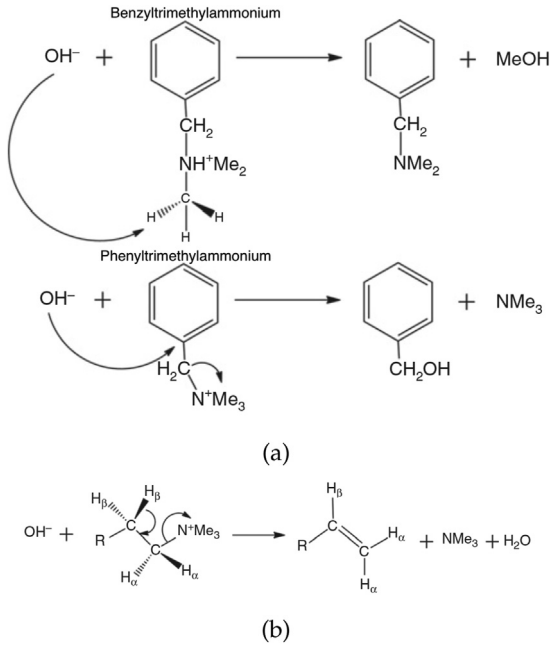


**Fig. 10 – (a) The direct nucleophilic substitution reactions, and (b) the Hoffman elimination reaction.**

chain cleavage and resulting mechanical degradation common to these types of backbones have been circumvented with AEM aryl backbones without ether-bonds [104,111]. Aryl ether-free AEM backbones can be approximated into two categories, aryl-aryl (poly(aryl piperidinium) (PAP) [111], polyphenylene [110], etc.) and alkyl-alkyl (polynorbornene [103,108,114], polyethylene [100,130], etc.) backbones. The latter generally displays higher peak power densities, a low solubility using most organic solvents and weak mechanical strength without PTFE-reinforcement (tensile strength ~10 MPa and > 200% elongation at break) compared to aryl-aryl backbone AEMs. AEMs based on aryl-aryl backbones do not require reinforcement having excellent mechanical strength (tensile strength > 60 MPa and 10–117% elongation at break).

A number of different strategies have been devised in recent years to overcome these issues, such as microphase separation, crosslinking and organic-inorganic composites [104]. Microphase separation is utilised in order to increase the performance of anionic membranes through augmenting their ionic conductivity and adjusting their dimensional stability. Crosslinking and organic-inorganic composites have been utilised with great success to alter the mechanical stability of an AEM.

The concept of microphase separation implies the backbone of the polymer is hydrophobic and the cation-containing polymer is hydrophilic [128,131]. In Nafion this is achieved by replacing the hydrogen atom with fluorine atoms in the main polymer chain, and non-fluorinated hydrocarbon-based polymers are used in AEMs. The microphase separation creates a region where water can be absorbed locally to improve the hydroxide ion conductivity while simultaneously controlling the amount of swelling that would otherwise degrade the mechanical strength. With this type of architecture AEMs can be fabricated with a higher anionic conductivity, while still possessing the same ion exchange capacity (IEC). There are 4 main types of AEM architectures that are based on microphase separation and these are shown in Fig. 11. These have contributed to great advancement in AEM performance in recent years.

In another approach a long alkyl chain was grafted onto a PPO backbone, forming a comb-like structure with microphase separation resulting in excellent stability maintaining 91% of its conductivity after a 700 h test in 2.0 M KOH at 60 °C despite the PPO backbone [119]. The comb-shaped morphology was considered responsible for the hydroxide conductivity (92.6/46.6 mS $cm^{-1}$ at 80/30 °C). Similarly, long side-chains are employed in an approach to induce microphase separation where using spacers which are chemically incorporated into polymer backbones to allow more room for the water of solvation to decrease swelling and mechanical degradation [132]. An aromatic AEM with a long pendant spacer exhibited a good ionic conductivity of 91 mS $cm^{-1}$ at 60 °C and virtually no degradation after 960 h in 6.0 M NaOH at 60 °C.

Several cationic groups were grafted onto a PES-backbone, where the 1-methylpyrrolidinium and 1-methylpiperidinium functionalised PES-AEMs displayed the greatest stability and AEMFC performance compared against two imidazoliums and a trimethylammonium at 60 °C in 2.0 M NaOH [121]. These results are in line with the degree of microphase separation. Limited R&D efforts are focused on PES, PEEK and polysulphone materials due to poor stability originating in the alkaline vulnerability of ether-bonds and poor FC performance (PPD ~109 mW $cm^{-2}$ at 60 °C).

Despite the several beneficial performances of AEMs with microphase separation there is still no evidence of causality between this method and in-situ AEMFC durability/peak power density [104].

With respect to functional cationic end-groups there are many approaches to making AEMs, including QA groups [103,108,119], quaternary phosphonium [117,126], imidazolium [115,122,124], guanidinium [123] and cobaltocenium [116]. Historically QAs have received more attention, however initial instability and manufacturing difficulties caused attention to swing towards the other options. Today QA groups are still widely employed in AEMs where initial stability issues have been ameliorated with techniques such as crosslinking [103,108].

Very light crosslinking was utilised in creating a breakthrough AEM. Synthesising a block copolymer-poly(norbornene) (BCP-PNB) through vinyl addition polymerisation with QA cation groups attached by pendant chains, with PTFE added for mechanical strength resulted in an AEM with a ionic conductivity of 212 mS $cm^{-1}$ at 80 °C [103]. The high performance of this AEM was partly attributed its very low thickness of 10 $\mu$m.

Creating an organic-inorganic composite by adding $TiO_2$, $SnO_2$, or layered double hydroxides as filler in AEMs represents another method for enhancing an AEMs mechanical properties [104,118]. The high ionic conductivity of 122 mS $cm^{-1}$ at 80 °C was recorded after spray-coating QA-functionalised layered double hydroxides (QA-LDH) onto the

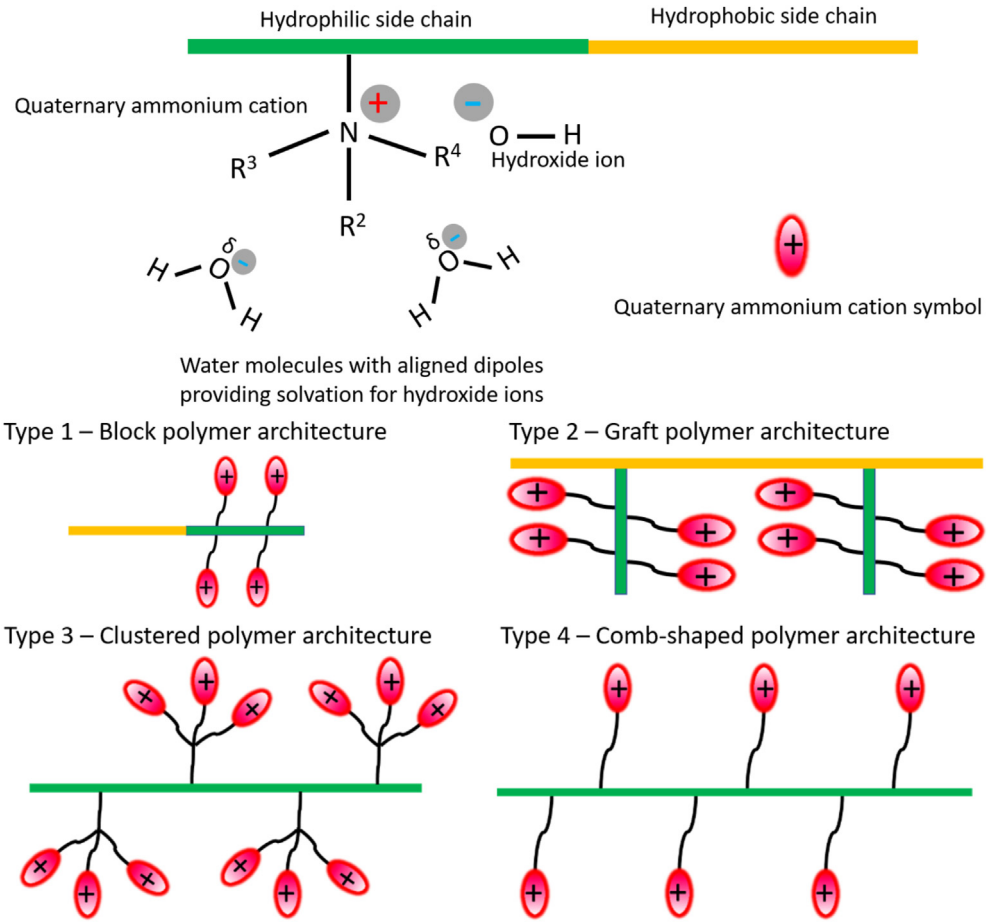


**Fig. 11 – AEM architectures based on microphase separation [128].**

surface of triple-ammonium side chain PPO membranes [118]. Due to inadequate fuel cell performance associated with this method, it has not garnered notable attention.

Recently, aryl ether-free PAP AEMs have amassed attention as stable, high-performance membranes [111]. PAP functionalised with biphenyl and terphenyl yielded stable AEMs with high ionic conductivities of 169 and 193 mS $cm^{-1}$ at 95 °C respectively. Moreover, both AEMs maintained their conductivity after 2000 h in 1.0 M NaOH at 100 °C in addition to displaying excellent mechanical qualities. Aryl ether-free PAP AEMs are currently being explored by many research groups. To decrease the adverse effects associated with phenyl groups, an aliphatic chain was integrated into a PAP AEM/ionomer resulting in aliphatic chain-containing poly(diphenylterphenyl piperidinium) (PDTP) copolymers [113]. Excellent mechanical and chemical stability was displayed with a tensile strength of 60–76 MPa and retaining 100% ionic conductivity after 1500 h in 1.0 M NaOH at 80 °C, in addition to great hydroxide conductivity of 158 mS $cm^{-1}$ at 60 °C.

Another aryl-aryl type polymer backbone that has shown great alkaline stability is polyphenylene [104,110]. Polyphenylene was functionalised with hexyltrimethylammonium (HTMA) and benzyltri methylammonium (BTMA) resulting in two AEMs [110]. Following an initial loss of conductivity within the first 100 h, the HTMA membrane retained its conductivity over 5300 h in both 0.5 and 2.0 M NaOH at 80 °C and surpassed the performance of the BTMA AEM. The stability test for the HTMA AEM was extended to 11,160 h, leaving the HTMA polyphenylene AEM with 28% of its initial hydroxide conductivity.

The realm of radiation grafted AEMs has been studied by Varcoe *et* al. for decades. Recently this group reported AEMs comprised of low density polyethylene (LDPE) yielding $OH^-$ conductivities in the region of 145 mS $cm^{-2}$ at 80 °C when fully hydrated [100]. A variant of this was used to make a high temperature AEMFC operating at 110 °C with a record high ionic conductivity of 300 mS $cm^{-1}$ at 110 °C [102]. More advanced versions of the LDPE membrane were compared against a high density polyethylene (HDPE) AEM, where the latter displayed a greater ionic conductivity (214 mS $cm^{-2}$ at 80 °C), smaller thicknesses and greater PPDs [130]. Similarly to the previously discussed aryl ether-free PAP AEMs, these AEMs possess poor microphase separation while still display great ex- and in-situ performance. This further underlines the lack of causality betweeen great AEMFC performance and microphase separation.

Membranes based on materials such as chitosan have attracted some attention in regard to sustainable AEM production. Chitosan is a non-toxic, bio-degradable cycloaliphatic polymer which contains hydroxide and active amino groups (-$NH_2$) on the polymer backbone which provide

hydrophilicity, high mechanical strength and chemical adaptability into the resulting membrane [124]. A chitosan and 1-ethenyl-3-methyl-1H-imidazoliumchloride polymer with 1-ethyl-2-pyrrolidone composites (CS/EMImC-Co-EP) were developed using a thermochemical crosslinking technique [124]. The membranes hydroxide conductivity remained stable following a 300 h test in a 8.0 M KOH solution at 85 °C. Crosslinking is necessary to increase the chemical and mechanical stability of chitosan while simultaneously rendering it insoluble in aqueous media. Sustainably produced AEMs have yet to yield matching performances to state of the art AEMs.

Several FC systems incorporate both an AEM and liquid electrolytes in an attempt to maintain long term performance and at the same time reduce gas crossover [93]. This latter idea has been embodied in a experimental AEM, using ion solvation polymers that absorb liquid alkalis such as KOH into their structure. A good example is polyvinyl alcohol that is crosslinked in the presence of strong KOH [133]. The initial AEM performance was good, but KOH is leached out with time due to the formation of water, removing $OH^-$ from the body of the polymer. However, this approach caused decreased $CO_2$ tolerance and the adverse formation of carbonate (Eq. (10)).

### *AEMFC performance and degradation*

The peak power densities (PPDs) of AEMFCs have advanced from mW $cm^{-2}$ to W $cm^{-2}$ and durabilities surpassing > 1000 h in the last decade. The current PPD and stability records paint a promising picture of AEMFC development, however there is a wide variation in PPDs as displayed in Table 4 where the performance of most AEMs in this review are featured. The highest PPD registered to date employs the previously mentioned PTFE-reinforced polynorbornene AEM, which produced 3.50 W $cm^{-2}$ at 80 °C, in addition to the very high current density of 9.7 A $cm^{-2}$ as shown in Fig. 12 [103]. Additionally, its durability was tested in-situ at 600 mA $cm^{-2}$ (~0.7

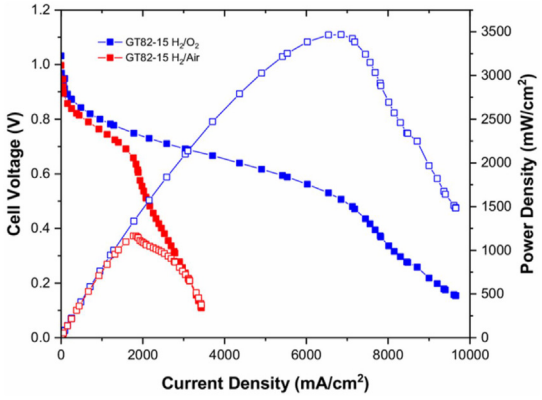


**Fig. 12 – Current-voltage and power curves displaying the highest power and current density achieved to date [103]. Optimised dew points, fuelled with $H_2/CO_2$-free air at 80 °C and anodic/cathodic metal loadings 0.70 $mg_{PtRu}$ $cm^{-2}$/0.60 $mg_{Pt}$ $cm^{-2}$ with 0.05/0.10 MPa back-pressure.**

**Table 4 – AEM fuel cell performances and associated performance-related aspects.*Only the Pt loading is specified, though a PtRu catalyst was employed.**

| Name [Company] | Power Density [mW $cm^{-2}$] | Catalyst (anode/cathode) [$mg_{metal}$ $cm^{-2}$] | Fuel | Back -pressure [MPa] |
|---|---|---|---|---|
| A-901 [Tokuyama] [107] | 450 (50 °C) | 0.50 (Pt)/0.50 (Pt) | $H_2/O_2$ | – |
| A-901 [Tokuyama] [107] | 340 (50 °C) | 0.50 (Pt)/0.50 (Pt) | $H_2/CO_2$-free air | – |
| Fumapem FAA-3-Br [FuMA – Tech] [135] | 428 (60 °C) | 0.40 (Pt)/0.50 (Pt) | $H_2/O_2$ | – |
| QA-LDH/TC-QAPPO [118] | 267 (60 °C) | 0.50 (Pt)/0.50 (Pt) | $H_2/O_2$ | 0.10/0.10 |
| PES-MPRD [121] | 109 (60 °C) | 0.50 (Pt)/0.50 (Pt) | $H_2/O_2$ | – |
| PES-MPY [121] | 106.5 (60 °C) | 0.50 (Pt)/0.50 (Pt) | $H_2/O_2$ | – |
| NCBP-Im [125] | 262 (50 °C) | 0.90 (Pt)/0.90 (Pt) | $H_2/O_2$ | – |
| PPO-AdIm-34 [120] | 46.0 (45 °C) | 0.80 (Pt)/0.80 (Pt) | $H_2/O_2$ | – |
| PSf-GIm-MImOH-130 [123] | 39.0 (50 °C) | 0.50 (Pt)/0.50 (Pt) | $H_2/O_2$ | – |
| CS/EMImC-Co-EP(1:0.5) [124] | 21.7 (25 °C) | 0.50 (Pt)/0.50 (Pt) | $H_2/O_2$ | – |
| GT82-15 [103] | 3500 (80 °C) | 0.70 (PtRu)/0.60 (Pt) | $H_2/O_2$ | 0.05/0.10 |
| GT64-15 [Xergy] [108] | 3370 (80 °C) | 0.70 (PtRu)/0.60 (Pt) | $H_2/O_2$ | – |
| PNB-$X_{62}$-$Y_{38}$ [114] | 542.6 (60 °C) | 1.05 (Pt)/1.05 (Pt) | $H_2/O_2$ | – |
| PVA-1.8PVBMP [101] | 1200 (60 °C) | 0.40 (PtRu)/2.0 ($FeN_x$-CNT) | $H_2/O_2$ | 0.10/0.10 |
| PAP-BP-60 [111] | 920 (95 °C) | 0.15 (Pt)/1.0 (Ag) | $H_2/CO_2$-free air | 0.25/0.13 |
| PDTP-25 [113] | 2580 80 °C) | 0.39 (PtRu)/0.26 (Pt) | $H_2/O_2$ | 0.13/0.13 |
| PDTP-25 [113] | 1380 80 °C) | 0.39 (PtRu)/0.26 (Pt) | $H_2/CO_2$-free air | 0.13/0.13<br>0.13/0.13 |
| LDPE-45$\mu$m [100] | 1450 (80 °C) | 0.40 (Pt)*/0.40(Pt) | $H_2/O_2$ | – |
| LDPE-45$\mu$m [100] | 931 (80 °C) | 0.40 (Pt)*/0.80 (Ag) | $H_2/O_2$ | – |
| LDPE-45$\mu$m [100,102] | 2100 (110 °C) | 0.70 (PtRu)/0.70 (Pt) | $H_2/O_2$ | 0.15/0.15 |
| LDPE-22$\mu$m [136] | 2020 (80 °C) | 0.40 (Pt)*/0.40 (Pt) | $H_2/O_2$ | – |
| LDPE-22$\mu$m [136] | 1620 (80 °C) | 0.40 (Pt)*/0.86 (Ag) | $H_2/O_2$ | – |
| LDPE-22$\mu$m [136] | 1260 (80 °C) | 0.40 (Pt)*/< 0.01 (FeCoPc) | $H_2/O_2$ | – |
| HDPE-21$\mu$m [130] | 2550 (80 °C) | 0.40 (Pt)*/0.40 (Pt) | $H_2/O_2$ | – |
| HPDE [130,134] | 2000 (80 °C) | 0.25 (Pd)/0.40 (Pt) | $H_2/O_2$ | – |
| HPDE [130,134] | 1000 (70 °C) | 0.25 (Pd)/0.03 (Fe) | $H_2/O_2$ | – |

$V_{RHE}$) at 80 °C over 545 h resulting in no significant degradation.

Such a high current density was possible due to the excellent water transport characteristics, in part afforded by the very low thickness of the AEM (10 $\mu$m).

An AEMFC utilising an PAP AEM yielded a PPD of 920 mW $cm^{-2}$ (fuelled with $H_2/CO_2$-free air at 95 °C with anodic/cathodic metal loadings 150 $\mu g_{Pt}$ $cm^{-2}$/1.0 $mg_{Ag}$ $cm^{-2}$ with 0.25/0.13 MPa back-pressure), and showed good stability with 11.5% voltage loss over 300 h (0.5 A $cm^{-2}$ (~0.65 V)) while fuelled with $H_2/CO_2$-free air at 95 °C [111]. A FC with a PAP with aliphatic chain AEM displayed a PPD of 2.58 W $cm^{-2}$ (fuelled with $H_2/O_2$ at 80 °C with anodic/cathodic metal loadings 0.39 $mg_{PtRu}$ $cm^{-2}$/0.26 $mg_{Pt}$ $cm^{-2}$ with 0.13/0.13 MPa back-pressure) [113].

Radiation grafted AEMFCs comprising low and high-density polyethylene AEMs were compared yielding PPDs of 2.01 and 2.55 W $cm^{-2}$ (fuelled with $H_2/O_2$ at 80 °C with anodic/cathodic metal loadings 0.40 $mg_{PtRu}$ $cm^{-2}$/0.40 $mg_{Pt}$ $cm^{-2}$ and no back-pressure) [130]. This increase in performance was accredited increased water transport due to the change in polyethylene. More importantly, the stability was greatly enhanced as shown by a 440 h durability test (0.60 A $cm^{-2}$ (~0.7 $V_{RHE}$), 70 °C with $H_2/CO_2$-free air) where the LDPE AEMFC was stopped after 100 h due to a large increase in area specific resistance. The AEMFC with LDPE and HDPE AEM yielded degradation rates of 790 and 68 $\mu V\ h^{-1}$ respectively.

The pre-discussed Pd–$CeO_2$/C HOR catalyst was employed as a substitute for PtRu and Pt in an AEMFC utilising a HPDE AEM with a variety of cathodes including Pd/C, Ag–Co/C, Fe/C and a Pt/C benchmark [134]. All cathodes with the Pd–$CeO_2$/C anode resulted in PPDs ≥1.0 W $cm^{-2}$, where the benchmark achieved a PPD of 2.0 W $cm^{-2}$ (fuelled with $H_2/O_2$ at 80 °C with anodic/cathodic metal loadings 0.25 mg $cm^{-2}_{Pd}$/0.4 $mg_{Pt}$ $cm^{-2}$ with no back-pressure) and the Fe/C a PPD of ~1.0 W $cm^{-2}$ (fuelled with $H_2/O_2$ at 70 °C with anodic/cathodic metal loadings 0.25 mg $cm^{-2}_{Pd}$/30 $\mu g_{Fe}$ $cm^{-2}$ with no back-pressure).

The radiation-grafted LDPE AEM described in Ref. [100] was employed in the first high-temperature AEMFC, which performed admirably at 110 °C, yielding a PPD of 2.1 W $cm^{-2}$ (fuelled with $H_2/O_2$ at 110 °C with anodic/cathodic metal loadings 0.70 $mg_{PtRu}$ $cm^{-2}$/0.70 $mg_{Pt}$ $cm^{-2}$ and 0.15/0.15 MPa back-pressure) [102]. High kinetic activity was exhibited through a high open circuit voltage (OCV) of 1.02 $V_{RHE}$ and a current density of 0.574 A $cm^{-2}$ (at 0.8 V), comparing most favourably against high-temperature PEMFCs (OCVs ≈ 0.95–0.96 $V_{RHE}$ and 70–300 mA $cm^{-2}$ at 0.8 $V_{RHE}$). Furthermore, the non-optimised high-temperature AEMFC was operated at 0.2 A $cm^{-2}$ for 50 h (same conditions as previously stated) with a fairly stable voltage producing an approximate degradation rate of 2 mV $h^{-1}$. Few long-term (>1000 h) AEMFC degradation rates have been reported. A half-cell (ORR) AEMFC was utilised to measure the stability of commercial 40 wt.%Pt/C, where a degradation rate of 29 $\mu V\ h^{-1}$ was reported after 1500 h at 0.31$V_{SHE}$ [137]. Fig. 13a shows one of the most recently reported degradation rates from 2020 [13], where a 5 $cm^2$ AEMFC utilising a PNB-type AEM operated for 2000 h with a very small voltage loss. Fig. 13b displays two AEMFC rates from 2011 to 2019, compared to the

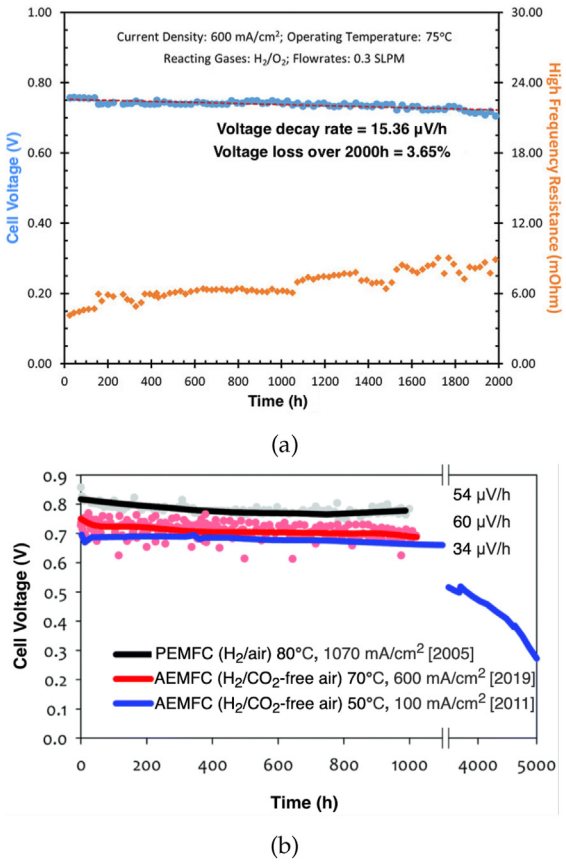


**Fig. 13 – (a) Cell voltage and high-frequency resistance during a long-term durability test [13]. Adapted with permission from John Wiley and Sons. (b) A durability comparison between two AEMFCs and a PEMFC, adapted from Ref. [11] with permission from The Royal Society of Chemistry.**

degradation rate of a PEMFC [11]. While the AEMFC degradation rate measured in 2011 (employing Tokuyama materials) is almost twice that of 2019, the increase in temperature and especially operating current density are most influential. Such a low rate of degradation despite these increases was made possible by employing a HDPE AEM and an EFTE ionomer. Furthermore, PO-CellTech reported a degradation rate of 7.5 $\mu V\ h^{-1}$ after 1400 h at 0.6 A $cm^{-2}$ at 75 °C, where this AEMFC was still running at the time of publication [11].

Water management is a critical challenge on the system level, as optimising this aspect can make a great difference to the performance of the AEMFC [103]. The current record-holder in AEMFC PPD labelled this facet as most critical, where rapid transport of water from the anode circumvents the issue of anodic catalyst flooding while simultaneously supplying water to the water-consuming cathode. Mechanical stability is of high importance in this regard, as producing very thin membranes enables fast water transport through the membrane and decreases the influence of the voltage drop across the membrane. Moreover, losses associated with poor water management are recoverable by increasing the dew points of the cell or by increasing the flow rate of the anode

[11]. The latter is impractical due to the expensive additional equipment required to sustain a high fuel efficiency. Further development of high-temperature AEMFCs will be deeply reliant on the experiences gained on this topic [102].

AEMFC degradation from a 100 h test under a variety of relative humidity (RH) conditions was recently investigated [138], where low anodic/cathodic RH (55%RH) induced a severe degradation of performance and failure after 20 h. The anode was most sensitive to low RHs and the most stable AEMFC was achieved with a 100%/50%RH anode/cathode. An anode with a low RH (50%/100%RH anode/cathode) caused a notable deterioration of performance, however adding 1.0 M NaOH into the FC resulted in reviving most of the FCs performance.

### *Ionomer development*

Development of anionic ionomer is a blooming field of study, where similarly to the present status of AEMs, an alkaline analogue to the familiar and well-known Nafion® products has not yet been created. While ionomers are often created by dissolving the AEM using a mixture of solvent and water (thus yielding an ionomer with a non-competing chemistry to the membrane), ionomers should ideally be developed separate from the AEM [11]. This is of great importance if the MEA preparation method requires a large difference in the solubility of the AEM and the ionomer. Due to the intrinsic characteristics of the anode/cathode, it is likely that optimised ionomers will be created separately from the AEM.

The ionomer-HOR catalyst interaction was studied, where the adsorption of ionomer components (phenyl groups) notably impacted on AEMFC anode performance [139]. Specifically, the co-adsorption of cation-hydroxide-water hindered the diffusion of hydrogen gas to the catalyst surface and phenyl-group adsorption filled active sites on the catalyst, effectively reducing its activity. Increasing the anode flow rate decreased the influence of co-adsorption, however considering the ionomer-catalyst interaction in the catalyst design this is solution if impractical. Design of ionomers less reliant on phenyl groups is a topic requiring further R&D.

The effect of these two issues were investigated and compared by altering a quaternised poly(biphenyl alkylene) ionomer through two different approaches to increase hydrogen access to the anode [140]. The first approach involved increasing the free volume in the quaternised poly(biphenyl alkylene) ionomer by inserting symmetric dimethyl groups into the backbone thereby increasing the hydrogen diffusion coefficient and also the PPD of the AEMFC by ~25%. Secondly, the functional group was changed from alkyl trimethylammonium to alkyl triethylammonium which resulted in a doubling of the hydrogen limiting current of the new ionomer in addition to increasing the PPD by 60% due to decreased co-adsorption and better hydrogen access to the surface of the catalyst. Co-adsorption of cation-hydroxide-water was therefore deemed as a superior source AEMFC performance degradation compared to slow diffusion of hydrogen gas due to phenyl adsorption.

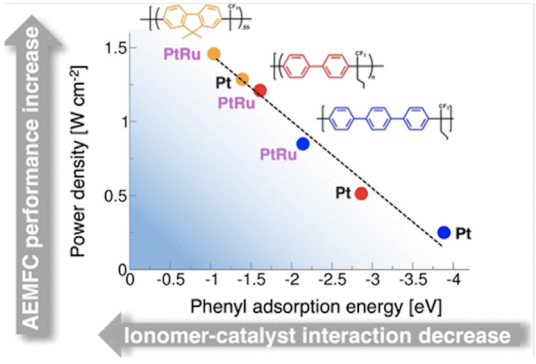


**Fig. 14 – AEMFC performance as a function of phenyl adsorption energy [141]. Reprinted with permission from Ref. [141]). Copyright (2021) American Chemical Society.**

A correlation between AEMFCs utilising Pt/PtRu catalysts and ionomers with various polyaromatic backbones was determined through DFT-determined adsorption energies of ionomer remnants onto metal [141]. As displayed in Fig. 14, AEMFC performance increases as the adsorption of phenyl groups weakens. Adsorption of benzene rings parallel to the catalyst metal surface causes a strong adsorption of ionomer fragments, and also a strong interaction and hybridisation of the aromatic $\pi$-orbitals with metal electronic states. The adsorption energies of the ionomers were determined as follows: p-terphenyl $\geq$ m-terphenyl > biphenyl > diphenyl ether > benzene $\geq$ o-terphenyl > 9,9- dimethyl fluorene. This study displays that use of fluorene-based ionomers such as FLN-55 should be prioritised over intermediate performing ones containing p-biphenylenes (BPN45 and BPN100) and especially the poorly performing p-TPN ionomer containing p-terphenyl remnants.

Generally speaking PtRu catalysts are less affected by phenyl groups, which is why this catalyst is generally preferred to Pt on the anode.

ORR catalysts can also be adversely affected by anionic ionomers as summarised in Ref. [107]. Ex-situ studies on the interaction between fully dissolved cations (free from a polymer) and Pt/C as an ORR catalyst exhibited that imidazolium cations caused a terrible degradation of performance, causing an increase in the production of peroxide-species. High potentials resulted in the Pt/C catalyst oxidising the organic ionomer, where the degradation products were harmful to both the ORR and the HOR. Furthermore, the ORR was scarcely affected by anionic ionomers comprising benzene ring-free QA cations like tetramethylammonium. Use of ionomers containing benzene rings, such as benzyltrimethylammonium lead to poor ORR performances.

A recent study optimised the ionomer, thereby doubling the power density (1.6 $\rightarrow$ 3.2 W $cm^{-2}$) [13]. This paper compared the tetrablock poly(norbornene) copolymers (GT32, GT64, GT78), where the excellent aforementioned performance increment was brought about by using a combination of these ionomers. By utilising the hydrophilic GT78 in the anode and the hydrophobic GT32 in the cathode, the characteristics of the ionomers harmonise with the intrinsic water requirements in the anode and cathode.

Ionomers with different ammonia concentrations were synthesised to optimise anodic/cathodic water management, thus enabling the AEMFC to operate under low RH [138]. Two quaternised poly(fluorene) (FLN) ionomers were

employed as binders in the creation of the MEAs, producing a comparable conclusion to Ref. [13], as using the more hydrophilic FLN-100 on anode side and FLN-55 on the cathode produced an improved AEMFC performance compared to most other configurations. Additionally, the two ionomers exhibited good alkaline stability with no structural changes after 720 h in 1.0 M NaOH at 80 °C. Low RH-conditions are attractive for automotive applications, however this imposes challenges for the ionomer [11]. The use of highly ionically conductive ionomers was suggested as an alleviating alternative.

The interaction between PGM/non-PGM catalysts (Pt/C, $Fe_{0.5}$-950 (HOR)/PtRu/C and Pd–$CeO_2$/C (ORR)) and a multitude of ionomers (Nafion (DuPont), FAA3 (FuMA-Tech) and 4 PPO-based anionic ionomers with different cationic groups) was investigated using a RDE [142]. Both Pt catalysts produced high activities with all ionomers and $Fe_{0.5}$-950 was highly efficient with the PPO-based ionomers compared to the commercial FAA3 ionomer. Generally, all catalyst-Nafion combinations resulted in greater diffusion limited current densities than any other ionomer. This was attributed to a lower $H_2/O_2$-permeability of the PPO-based ionomers and/or an incomplete ion-exchange (converting the PPO ionomers from bromide to hydroxide form).

Moreover, the 4 PPO-based anionic ionomers were designed free of fluorine, which similarly to using chitosan for creating AEMs [124,143] will be a meaningful aspect in regard to the environmental friendliness of AEMFC technology.

### *Summary*

Great advancements in polymer science has resulted in highly conductive and mechanically stable AEM classes such as PNB, PAP and HDPE. Advancements such as these have engendered great AEMFC performances with notable durability. Both in- and ex-situ experiments have been effective in mapping out issues and determining solutions such as characterising the ionomer-catalyst relationship, though additional advancements on these topics is necessary. Comparing the featured degradation rates of AFCs and AEMFCs in regard to their maturity tells the tale of the progress AEMFC technology has undergone. However, it is important to note the average rate of degradation for AEMFCs is notably higher (~500 $\mu V\ h^{-1}$), and accounting for these rates renders AEMFCs more typical of a technology at the beginning of its life.

## Conclusion and outlook

Having gained a significant amount of attention, the progress of AEMFCs over the last five years has been momentous. Numerous challenges remain on all levels, from the chemical/mechanical stability of the AEM and the interaction between the ionomer and the catalyst on the component level, to issues such as water management and carbonate build-up on the system level. The realisation of AEMFCs with PPDs > 1.0 W $cm^{-2}$ operating at > 1000 h with low degradation rates (~5–10 $\mu V\ h^{-1}$) paints a promising picture, however these targets will initially have to be met again with ultra-low PGM loadings (<100 $\mu g\ cm^{-2}$) to capture and keep commercial interest and prove the viability of AEM technology compared to PEMFCs. Further on, these targets must be met a third time with a non-PGM AEMFC. The following points represent some of the main R&D areas. Correctly addressing the following comprehensive challenges will require cooperation between industry and academia.

- Creating efficient and stable HOR/ORR non-PGM catalysts able to match or surpass the performance of the PGM benchmark. While encouraging performances with TM-based and heteroatom-doped materials have been reported, a significant body of work remains on this topic, specifically in regard to long-term stability (>1000 h).
- AEM performance has increased notably, though a performance which satisfies the rigorous demands has yet to be demonstrated. Similarly to catalyst development, stability is the principal barrier to overcome for AEMs also.
- Few large-scale (>100 $cm^2$) AEMFCs have been built, hence further efforts are required to face the optimisation challenges on the system level.
- Overall, streamlined design strategies are required for catalysts, ionomer, electrolyte and miscellaneous electrode components to avoid a mismatch of electrochemical properties.

Achieving the performance goals outlined by the US DOE [12] represents the first step only, as further progress yet is required. Each of these bullet points are composite challenges where every facet (e.g. AEM, ionomer, catalyst and its support, MEA components and preparation, FC fuel, dew points, etc.) requires optimisation. Realising AEMFCs as a cog in the future hydrogen economy is contingent on solving these challenges if they are to take their envisioned role in the global energy transition.

## Declaration of competing interest

The authors declare that they have no known competing financial interests or personal relationships that could have appeared to influence the work reported in this paper.

## REFERENCES

[1] Pivnyak G, Beshta O, Alekseyev M. Power engineering and information technologies in technical objects control: 2016 annual proceedings. CRC Press; 2017.
[2] Firouzjaie HA, Mustain WE. Catalytic advantages, challenges, and priorities in alkaline membrane fuel cells. 2019.
[3] AFC energy plc. AFC energy plc - admission to AIM - first day of dealings. Online; 2007. https://www2.trustnet.com/Investments/Article. aspx?id=200704240801013820 V.
[4] Brandon NNP, Thompsett D. Fuel cells compendium. Elsevier; 2005.
[5] Bidault F, Middleton PH. Comprehensive renewable energy. In: Chapter 4.07 Alkaline fuel cells: theory and application, vol. 1. Elsevier; 2012.
[6] McLean GF, Niet T, Prince-Richard S, Djilali N. An assessment of alkaline fuel cell technology. Int J Hydrogen Energy 2002;27(5):507–26.

[7] Kiros Y, Myrén C, Schwartz S, Sampathrajan A, Ramanathan M. Electrode r&d, stack design and performance of biomass-based alkaline fuel cell module. Int J Hydrogen Energy 1999;24:549–64.
[8] Kiros Y, Schwartz S. Long-term hydrogen oxidation catalysts in alkaline fuel cells. J Power Sources 2000;87(1):101–5.
[9] Sato M, Ohta M, Sakaguchi M. Effect of carbon dioxide on electrochemical stability of gas diffusion electrodes in alkaline solution. Electrochim Acta 1990;35(6):945–50.
[10] Gouérec P, Poletto L, Denizot J, Sanchez-Cortezon E, Miners JH. The evolution of the performance of alkaline fuel cells with circulating electrolyte. J Power Sources 2004;129(2):193–204.
[11] Mustain WE, Chatenet M, Page M, Kim YS. Durability challenges of anion exchange membrane fuel cells. Energy Environ Sci 2020;13(9):2805–38.
[12] Gottesfeld S, Dekel DR, Page M, Bae C, Yan Y, Zelenay P, Kim YS. Anion exchange membrane fuel cells: current status and remaining challenges. J Power Sources 2018;375:170–84.
[13] Ul Hassan N, Mandal M, Huang G, Firouzjaie HA, Kohl PA, Mustain WE. Achieving high-performance and 2000 h stability in anion exchange membrane fuel cells by manipulating ionomer properties and electrode optimization. Adv Energy Mat 2020;10(40):2001986.
[14] Firouzjaie HA, Mustain WE. Catalytic advantages, challenges, and priorities in alkaline membrane fuel cells. ACS Catal 2020;10(1):225–34.
[15] Yang F, Bao X, Zhao Y, Wang X, Cheng G, Luo W. Enhanced HOR catalytic activity of PGM-free catalysts in alkaline media: the electronic effect induced by different heteroatom doped carbon supports. J Mater Chem A 2019;7(18):10936–41.
[16] Cong Y, Yi B, Song Y. Hydrogen oxidation reaction in alkaline media: from mechanism to recent electrocatalysts. Nano Energy 2018;44:288–303.
[17] Paraknowitsch JP, Thomas A. Doping carbons beyond nitrogen: an overview of advanced heteroatom doped carbons with boron, sulphur and phosphorus for energy applications. Energy Environ Sci 2013;6(10):2839–55.
[18] Liu X, Dai L. Carbon-based metal-free catalysts. Nat Rev Mat 2016;1(11):1–12.
[19] Ge X, Sumboja A, Wuu D, An T, Li B, Goh FWT, Hor TSA, Zong Y, Liu Z. Oxygen reduction in alkaline media: from mechanisms to recent advances of catalysts. ACS Catal 2015;5(8):4643–67.
[20] Schmidt TJ, Stamenkovic V, Arenz M, Markovic NM, Ross Jr PN. Oxygen electrocatalysis in alkaline electrolyte: Pt (hkl), Au (hkl) and the effect of Pd-modification. Electrochim Acta 2002;47(22–23):3765–76.
[21] Sheng W, Gasteiger HA, Shao-Horn Y. Hydrogen oxidation and evolution reaction kinetics on platinum: acid vs alkaline electrolytes. J Electrochem Soc 2010;157(11):B1529–36.
[22] Rossmeisl J, Chan K, Skulason E, Björketun ME, Tripkovic V. On the pH dependence of electrochemical proton transfer barriers. Catal Today 2016;262:36–40.
[23] Zheng J, Sheng W, Zhuang Z, Xu B, Yan Y. Universal dependence of hydrogen oxidation and evolution reaction activity of platinum-group metals on ph and hydrogen binding energy. Sci Adv 2016;2(3):e1501602.
[24] Subbaraman R, Tripkovic D, Chang K-C, Strmcnik D, Paulikas AP, Hirunsit P, Chan M, Greeley J, Stamenkovic V, Markovic NM. Trends in activity for the water electrolyser reactions on 3d-M(Ni, Co, Fe, Mn)-hydr(oxy)oxide catalysts. Nat Mater 2012;11(6):550–7.
[25] Sun Y, Dai Y, Liu Y, Chen S. A rotating disk electrode study of the particle size effects of Pt for the hydrogen oxidation reaction. Phys Chem Chem Phys 2012;14(7):2278–85.
[26] Schmidt TJ, Ross Jr PN, Markovic NM. Temperature dependent surface electrochemistry on Pt single crystals in alkaline electrolytes: Part 2. The hydrogen evolution/oxidation reaction. J Electroanal Chem 2002;524:252–60.
[27] Ohyama J, Sato T, Yamamoto Y, Arai S, Satsuma A. Size specifically high activity of Ru nanoparticles for hydrogen oxidation reaction in alkaline electrolyte. J Am Chem Soc 2013;135(21):8016–21.
[28] Scofield ME, Zhou Y, Yue S, Wang L, Su D, Tong X, Vukmirovic MB, Adzic RR, Wong SS. Role of chemical composition in the enhanced catalytic activity of pt-based alloyed ultrathin nanowires for the hydrogen oxidation reaction under alkaline conditions. ACS Catal 2016;6(6):3895–908.
[29] Gao X, Wang Y, Xie H, Liu T, Chu W. High activity of a Pt decorated Ni/C nanocatalyst for hydrogen oxidation. Chin J Catal 2017;38(2):396–403.
[30] Antolini E. Palladium in fuel cell catalysis. Energy Environ Sci 2009;2(9):915–31.
[31] Henning S, Herranz J, Gasteiger HA. Bulk-palladium and palladium-on-gold electrocatalysts for the oxidation of hydrogen in alkaline electrolyte. J Electrochem Soc 2015;162(1):F178–89.
[32] Bellini M, Pagliaro MV, Lenarda A, Fornasiero P, Marelli M, Evangelisti C, Innocenti M, Jia Q, Mukerjee S, Jankovic J, et al. Palladium-ceria catalysts with enhanced alkaline hydrogen oxidation activity for anion exchange membrane fuel cells. ACS Appl Energy Mater 2019;2(7):4999–5008.
[33] Wang H, D Abruña H. Irpdru/c as $h_2$ oxidation catalysts for alkaline fuel cells. J Am Chem Soc 2017;139(20):6807–10.
[34] Schultze K, Bartelt H. Formation and reduction of nickel (II) hydroxide on Raney-nickel electrodes and its influence on the hydrogen overvoltage. Int J Hydrogen Energy 1992;17(9):711–8.
[35] Davydova ES, Mukerjee S, ic Jaouen F, Dekel DR. Electrocatalysts for hydrogen oxidation reaction in alkaline electrolytes. ACS Catal 2018;8(7):6665–90.
[36] Ewe H, Justi E, Schmitt A. Struktur und eigenschaften von Raney-Nickel-katalysatoren mit zulegierungen für alkalische brennstoffzellen. Electrochim Acta 1974;19(12):799–808.
[37] Lu S, Pan J, Huang A, Zhuang L, Lu J. Alkaline polymer electrolyte fuel cells completely free from noble metal catalysts. Proc Natl Acad Sci Unit States Am 2008;105(52):20611–4.
[38] Al-Saleh MA, Gultekin S, Al-Zakri AS, Khan AAA. Steady state performance of copper impregnated Ni/PTFE gas diffusion electrode in alkaline fuel cell. Int J Hydrogen Energy 1996;21(8):657–61.
[39] Oshchepkov AG, Bonnefont A, Pronkin SN, Cherstiouk OV, Ulhaq-Bouillet C, Papaefthimiou V, Parmon VN, Savinova ER. Nanostructured nickel nanoparticles supported on vulcan carbon as a highly active catalyst for the hydrogen oxidation reaction in alkaline media. J Power Sources 2018;402:447–52.
[40] Kabir S, Lemire K, Artyushkova K, Roy A, Odgaard M, Schlueter D, Oshchepkov A, Bonnefont A, Savinova E, Sabarirajan DC, et al. Platinum group metal-free nimo hydrogen oxidation catalysts: high performance and durability in alkaline exchange membrane fuel cells. J Mater Chem A 2017;5(46):24433–43.
[41] Wang G, Li W, Huang B, Xiao L, Lu J, Zhuang L. Exploring the composition–activity relation of Ni-Cu binary alloy

electrocatalysts for hydrogen oxidation reaction in alkaline media. ACS Appl Energy Mater 2019;2(5):3160–5.
[42] Davydova ES, Zaffran J, Dhaka K, Toroker MC, Dekel DR. Hydrogen oxidation on ni-based electrocatalysts: the effect of metal doping. Catalysts 2018;8(10):454.
[43] Davydova ES, Speck FD, Paul MTY, Dekel DR, Cherevko S. Stability limits of ni-based hydrogen oxidation electrocatalysts for anion exchange membrane fuel cells. ACS Catal 2019;9(8):6837–45.
[44] Sheng W, Bivens AP, Myint M, Zhuang Z, Forest RV, Fang Q, Chen JG, Yan Y. Non-precious metal electrocatalysts with high activity for hydrogen oxidation reaction in alkaline electrolytes. Energy Environ Sci 2014;7(5):1719–24.
[45] Ni W, Krammer A, Hsu C-S, Chen HM, Schüler A, Hu X. $Ni_3N$ as an active hydrogen oxidation reaction catalyst in alkaline medium. Angew Chem Int Ed 2019;58(22):7445–9.
[46] Song F, Li W, Yang J, Han G, Liao P, Sun Y. Interfacing nickel nitride and nickel boosts both electrocatalytic hydrogen evolution and oxidation reactions. Nat Commun 2018;9(1):1–10.
[47] Zhuang Z, Giles SA, Zheng J, Jenness GR, Caratzoulas S, Vlachos DG, Yan Y. Nickel supported on nitrogen-doped carbon nanotubes as hydrogen oxidation reaction catalyst in alkaline electrolyte. Nat Commun 2016;7(1):1–8.
[48] Zhou Z, Liu Y, Zhang J, Pang H, Zhu G. Non-precious nickel-based catalysts for hydrogen oxidation reaction in alkaline electrolyte. Electrochem Commun 2020;121:106871.
[49] Durst J, Siebel A, Simon C, Hasche F, Herranz J, Gasteiger HA. New insights into the electrochemical hydrogen oxidation and evolution reaction mechanism. Energy Environ Sci 2014;7(7):2255–60.
[50] Sarkar S, Patel S, Sampath S. Efficient oxygen reduction activity on layered palladium phosphosulphide and its application in alkaline fuel cells. J Power Sources 2020;445:227280.
[51] B Lima FH, Ticianelli EA. Oxygen electrocatalysis on ultra-thin porous coating rotating ring/disk platinum and platinum–cobalt electrodes in alkaline media. Electrochim Acta 2004;49(24):4091–9.
[52] Ramesh KV, Shukla AK. Carbon-based electrodes carrying platinum-group bimetal catalysts for oxygen reduction in fuel cells with acidic or alkaline electrolytes. J Power Sources 1987;19(4):279–85.
[53] Ren X, Lv Q, Liu L, Liu B, Wang Y, Liu A, Wu G. Current progress of Pt and Pt-based electrocatalysts used for fuel cells. Sustain Energy Fuels 2020;4(1):15–30.
[54] Shao M, Liu P, Zhang J, Adzic R. Origin of enhanced activity in palladium alloy electrocatalysts for oxygen reduction reaction. J Phys Chem B 2007;111(24):6772–5.
[55] Wang Y, Balbuena PB. Design of oxygen reduction bimetallic catalysts: ab-initio-derived thermodynamic guidelines. J Phys Chem B 2005;109(40):18902–6.
[56] Erikson H, Sarapuu A, Alexeyeva N, Tammeveski K, Solla-Gullón J, Feliu JM. Electrochemical reduction of oxygen on palladium nanocubes in acid and alkaline solutions. Electrochim Acta 2012;59:329–35.
[57] Jiang L, Hsu A, Chu D, Chen R. Size-dependent activity of palladium nanoparticles for oxygen electroreduction in alkaline solutions. J Electrochem Soc 2009;156(5):B643–9.
[58] Jukk K, Alexeyeva N, Ritslaid P, Kozlova J, Sammelselg V, Tammeveski K. Electrochemical reduction of oxygen on heat-treated pd nanoparticle/multi-walled carbon nanotube composites in alkaline solution. Electrocatalysis 2013;4(1):42–8.
[59] Adžić RR, Strbac S, Anastasijević N. Electrocatalysis of oxygen on single crystal gold electrodes. Mater Chem Phys 1989;22(3):349–75.
[60] Marković NM, Adžić RR, Cahan BD, Yeager EB. Structural effects in electrocatalysis: oxygen reduction on platinum low index single-crystal surfaces in perchloric acid solutions. J Electroanal Chem 1994;377(1–2):249–59.
[61] Lu F, Zhang Y, Liu S, Lu D, Su D, Liu M, Zhang Y, Liu P, Wang JX, Adzic RR, et al. Surface proton transfer promotes four-electron oxygen reduction on gold nanocrystal surfaces in alkaline solution. J Am Chem Soc 2017;139(21):7310–7.
[62] Hu P, Song Y, Chen L, Chen S. Electrocatalytic activity of alkyne-functionalized agau alloy nanoparticles for oxygen reduction in alkaline media. Nanoscale 2015;7(21):9627–36.
[63] Gong H, Zhang W, Li F, Yang R. Enhanced electrocatalytic performance of self-supported AuCuCo for oxygen reduction and evolution reactions. Electrochim Acta 2017;252:261–7.
[64] Kostowskyj MA, Gilliam RJ, Kirk DW, Thorpe SJ. Silver nanowire catalysts for alkaline fuel cells. Int J Hydrogen Energy 2008;33(20):5773–8.
[65] Coutanceau C, Demarconnay L, Lamy C, Léger JM. Development of electrocatalysts for solid alkaline fuel cell (SAFC). J Power Sources 2006;156(1):14–9.
[66] Guan W, Zhang L, Fan X, Shi Z, Wang Q, Cui X, Zheng W. Shape-dependent catalytic activity of oxygen reduction reaction (ORR) on silver nanodecahedra and nanocubes. J Power Sources 2014;269:152–7.
[67] Qiu Z, Huang N, Ge X, Xuan J, Wang P. Preparation of N-doped nano-hollow capsule carbon nanocage as ORR catalyst in alkaline solution by PVP modified F127. Int J Hydrogen Energy 2020;45(15):8667–75.
[68] Li B, Sasikala SP, Kim DH, Bak J, Kim I-D, Cho E, Kim SO. Fe-n4 complex embedded free-standing carbon fabric catalysts for higher performance orr both in alkaline & acidic media. Nano energy 2019;56:524–30.
[69] Hanif S, Iqbal N, Shi X, Noor T, Ali G, Kannan AM. NiCo-N-doped carbon nanotubes based cathode catalyst for alkaline membrane fuel cell. Renew Energy 2020;154:508–16.
[70] Yuan K, Sfaelou S, Qiu M, Lutzenkirchen-Hecht D, Zhuang X, Chen Y, Yuan C, Feng X, Scherf U. Synergetic contribution of boron and Fe-$N_x$ species in porous carbons toward efficient electrocatalysts for oxygen reduction reaction. ACS Energy Letters 2017;3(1):252–60.
[71] Sun Y, Wu J, Tian J, Jin C, Yang R. Sulfur-doped carbon spheres as efficient metal-free electrocatalysts for oxygen reduction reaction. Electrochim Acta 2015;178:806–12.
[72] Wu J, Jin C, Yang Z, Tian J, Yang R. Synthesis of phosphorus-doped carbon hollow spheres as efficient metal-free electrocatalysts for oxygen reduction. Carbon 2015;82:562–71.
[73] Ortiz J, Gautier JL. Oxygen reduction on copper chromium manganites. Effect of oxide composition on the reaction mechanism in alkaline solution. J Electroanal Chem 1995;391(1–2):111–8.
[74] Rios E, Reyes H, Ortiz J, Gautier JL. Double channel electrode flow cell application to the study of $\mathrm{HO}_2^-$ production on $Mn_xCo_{3-x}O_4$ ($0 \leq x \leq 1$) spinel films. Electrochim Acta 2005;50(13):2705–11.
[75] Trasatti S. Electrocatalysis in the anodic evolution of oxygen and chlorine. Electrochim Acta 1984;29(11):1503–12.
[76] Liang Y, Li Y, Wang H, Zhou J, Wang J, Regier T, Dai H. $Co_3O_4$ nanocrystals on graphene as a synergistic catalyst for oxygen reduction reaction. Nat Mater 2011;10(10):780–6.
[77] Cook WR, Jaffe B, Jaffe H. Piezoelectric ceramics, vol. 3. Elsevier; 2012.
[78] Suntivich J, Gasteiger HA, Yabuuchi N, Nakanishi H, Goodenough JB, Shao-Horn Y. Design principles for oxygen-reduction activity on perovskite oxide catalysts for fuel cells and metal-air batteries. Nat Chem 2011;3(7):546–50.

[79] Xu M, Sun H, Wang W, Shen Y, Zhou W, Wang J, Chen Z-G, Shao Z. Scandium and phosphorus co-doped perovskite oxides as high-performance electrocatalysts for the oxygen reduction reaction in an alkaline solution. J Mater Sci Technol 2020;39(22–27).
[80] Osgood H, Devaguptapu SV, Xu H, Cho J, Wu G. Transition metal (Fe, Co, Ni, and Mn) oxides for oxygen reduction and evolution bifunctional catalysts in alkaline media. Nano Today 2016;11(5):601–25.
[81] Meng Y, Song W, Huang H, Ren Z, Chen S-Y, Suib SL. Structure-property relationship of bifunctional $MnO_2$ nanostructures: highly efficient, ultra-stable electrochemical water oxidation and oxygen reduction reaction catalysts identified in alkaline media. J Am Chem Soc 2014;136(32):11452–64.
[82] Tomantschger K, McClusky F, Oporto L, Reid A, Kordesch K. Development of low cost alkaline fuel cells. J Power Sources 1986;18(4):317–35.
[83] Ma J, Sahai Y. Effect of electrode fabrication method and substrate material on performance of alkaline fuel cells. Electrochem Commun 2013;30:63–6.
[84] Bidault F, Brett DJL, Middleton PH, Abson N, Brandon NP. A new application for nickel foam in alkaline fuel cells. Int J Hydrogen Energy 2009;34(16):6799–808. 4th Dubrovnik Conference.
[85] Chen J, Zheng H, Kang J, Yang F, Cao Y, Xiang M. An alkaline direct oxidation glucose fuel cell using three-dimensional structural au/ni-foam as catalytic electrodes. RSC Adv 2017;7(5):3035–42.
[86] Kiros Y, Schwartz S. Pyrolyzed macrocycles on high surface area carbons for the reduction of oxygen in alkaline fuel cells. J Power Sources 1991;36(4):547–55.
[87] Pirjamali M, Kiros Y. Effects of carbon pretreatment for oxygen reduction in alkaline electrolyte. J Power Sources 2002;109(2):446–51.
[88] Brandon NP, Brett DJ. Engineering porous materials for fuel cell applications. Phil Trans Math Phys Eng Sci 2006;364(1838):147–59.
[89] Tomantschger K, Kordesch KV. Structural analysis of alkaline fuel cell electrodes and electrode materials. J Power Sources 1989;25(3):195–214.
[90] Li YS, Zhao TS. A high-performance integrated electrode for anion-exchange membrane direct ethanol fuel cells. Int J Hydrogen Energy 2011;36(13):7707–13. Hysydays.
[91] Bidault F, Kucernak A. Cathode development for alkaline fuel cells based on a porous silver membrane. J Power Sources 2011;196(11):4950–6.
[92] Tiwari P, Tsekouras G, Swiegers GF, Wallace GG. Gortex-based gas diffusion electrodes with unprecedented resistance to flooding and leaking. ACS Appl Mater Interfaces 2018;10(33):28176–86.
[93] Omasta TJ, Zhang Y, Park AM, Peng X, Pivovar B, Varcoe JR, Mustain WE. Strategies for reducing the PGM loading in high power AEMFC anodes. J Electrochem Soc 2018;165(9):F710.
[94] Gülzow E, Schulze M. Long-term operation of AFC electrodes with $CO_2$ containing gases. J Power Sources 2004;127(1–2):243–51.
[95] Tomantschger K, Findlay R, Hanson M, Kordesch K, Srinivasan S. Degradation modes of alkaline fuel cells and their components. J Power Sources 1992;39(1):21–41.
[96] Zadick A, Dubau L, Sergent N, Berthome G, Chatenet M. Huge instability of Pt/C catalysts in alkaline medium. ACS Catal 2015;5(8):4819–24.
[97] Burchardt T, Gouérec P, Sanchez-Cortezon E, Karichev Z, Miners JH. Alkaline fuel cells: contemporary advancement and limitations. Fuel 2002;81(17):2151–5.
[98] Vielstich W, Lamm A, Gasteiger HA. Handbook of fuel cells: fundamentals, technology and applications, vol. 2. New York: Wiley; 2003.
[99] Brown T. Gencell launches commercial alkaline fuel cell using cracked ammonia fuel. jul 2018. https://www.ammoniaenergy.org/articles/gencell-launches-commercial-alkaline-fuel-cell-using-cracked-ammonia-fuel/.
[100] Wang L, Brink JJ, Liu Y, Herring AM, Ponce-González J, Whelligan DK, Varcoe JR. Non-fluorinated pre-irradiation-grafted (peroxidated) LDPE-based anion-exchange membranes with high performance and stability. Energy Environ Sci 2017;10(10):2154–67.
[101] Zeng L, He Q, Liao Y, Kuang S, Wang J, Ding W, Liao Q, Wei Z, et al. Anion exchange membrane based on interpenetrating polymer network with ultrahigh ion conductivity and excellent stability for alkaline fuel cell. Research 2020;4794706:2020.
[102] Douglin JC, Varcoe JR, Dekel DR. A high-temperature anion-exchange membrane fuel cell. J Power Sources Adv 2020;5:100023.
[103] Mandal M, Huang G, Ul Hassan N, Peng X, Gu T, Brooks-Starks AH, Bahar B, Mustain WE, Kohl PA. The importance of water transport in high conductivity and high-power alkaline fuel cells. J Electrochem Soc 2019;167(5):054501.
[104] Chen N, Lee YM. Anion exchange polyelectrolytes for membranes and ionomers. Prog Polym Sci 2021;113:101345.
[105] Merle G, Wessling M, Nijmeijer K. Anion exchange membranes for alkaline fuel cells: a review. J Membr Sci 2011;377(1–2):1–35.
[106] Kim DJ, Jeong MK, Nam SY. Research trends in ion exchange membrane processes and practical applications. Appl Chem Eng 2015;26(1):1–16.
[107] Varcoe JR, Atanassov P, Dekel DR, Herring AM, Hickner MA, Kohl PA, Kucernak AR, Mustain WE, Nijmeijer K, Scott K, Xu T, Zhuang L. Anion-exchange membranes in electrochemical energy systems. Energy Environ Sci 2014;7(10):3135–91.
[108] Huang G, Mandal M, Peng X, Yang-Neyerlin AC, Pivovar BS, Mustain WE, Kohl PA. Composite poly (norbornene) anion conducting membranes for achieving durability, water management and high power (3.4 w/$cm^2$) in hydrogen/oxygen alkaline fuel cells. J Electrochem Soc 2019;166(10):F637.
[109] Xergy Inc. XIONTM composite – AEM - pention - 72 - 15CL-05μm. https://www..xergyincstore.com; jul 2020. https://www.xergyincstore.com/shop/xion-composite-ion-exchange-membrane/xion-aem/pention/xion-composite-pention-aem-72-15cl-05%CE%BCm/.
[110] Park EJ, Maurya S, Hibbs MR, Fujimoto CH, Kreuer K-D, Kim YS. Alkaline stability of quaternized diels–alder polyphenylenes. Macromolecules 2019;52(14):5419–28.
[111] Wang J, Zhao Y, Setzler BP, Rojas-Carbonell S, Yehuda CB, Amel A, Page M, Wang L, Hu K, Shi L, et al. Poly(aryl piperidinium) membranes and ionomers for hydroxide exchange membrane fuel cells. Nat Energy 2019;4(5):392–8.
[112] Olsson JS, Pham TH, Jannasch P. Poly(arylene piperidinium) hydroxide ion exchange membranes: synthesis, alkaline stability, and conductivity. Adv Funct Mater 2018;28(2):1702758.
[113] Lee YM, Chen N, Hu C, Wang HH, Kim SP, Kim HM, Lee WH, Bae JY, Park JH. Poly(alkyl-terphenyl piperidinium) ionomers and membranes with outstanding alkaline membrane fuel cell performance of 2.58 w $cm^{-2}$. Angew Chem Int Ed 2021;60(4):7710–8.
[114] Mandal M, Huang G, Kohl PA. Anionic multiblock copolymer membrane based on vinyl addition polymerization of

norbornenes: applications in anion-exchange membrane fuel cells. J Membr Sci 2019;570:394–402.
[115] Lee B-N, Son TY, Park CH, Kim TH, Nam SY. Preparation and characterization of various poly (ether ether ketone) containing imidazolium moiety for anion exchange membrane fuel cell application. J Nanosci Nanotechnol 2018;18(9):6447–54.
[116] Zhu T, Xu S, Rahman A, Dogdibegovic E, Yang P, Pageni P, Kabir MP, Zhou X-D, Tang C. Cationic metallo-polyelectrolytes for robust alkaline anion-exchange membranes. Angew Chem 2018;130(9):2412–6.
[117] Noonan KJT, Hugar KM, Kostalik IV HA, Lobkovsky EB, Abrunña HD, Coates GW. Phosphonium-functionalized polyethylene: a new class of base-stable alkaline anion exchange membranes. J Am Chem Soc 2012;134(44):18161–4.
[118] Chen N, Long C, Li Y, Wang D, Zhu H. High-performance layered double hydroxide/poly (2, 6-dimethyl-1, 4-phenylene oxide) membrane with porous sandwich structure for anion exchange membrane fuel cell applications. J Membr Sci 2018;552:51–60.
[119] Shukla G, Shahi VK. Well-designed mono-and di-functionalized comb-shaped poly (2,6-dimethylphenylene oxide) based alkaline stable anion exchange membrane for fuel cells. Int J Hydrogen Energy 2018;43(47):21742–9.
[120] Wang J, Wang X, Zu D, Hua Y, Li Y, Yang S, Wei H, Ding Y. N3-adamantyl imidazolium cations: alkaline stability assessment and the corresponding comb-shaped anion exchange membranes. J Membr Sci 2018;545:116–25.
[121] Liu FH, Lin CX, Hu EN, Yang Q, Zhang QG, Zhu AM, Liu QL. Anion exchange membranes with well-developed conductive channels: effect of the functional groups. J Membr Sci 2018;564:298–307.
[122] Zhang F, Zhang H, Qu C. Imidazolium functionalized polysulfone anion exchange membrane for fuel cell application. J Mater Chem 2011;21(34):12744–52.
[123] Cheng J, Yang G, Zhang K, He G, Jia J, Yu H, Gai F, Li L, Hao C, Zhang F. Guanidimidazole-quanternized and cross-linked alkaline polymer electrolyte membrane for fuel cell application. J Membr Sci 2016;501:100–8.
[124] Song F, Fu Y, Gao Y, Li J, Qiao J, Zhou X-D, Liu Y. Novel alkaline anion-exchange membranes based on chitosan/ethenylmethylimidazoliumchloride polymer with ethenylpyrrolidone composites for low temperature polymer electrolyte fuel cells. Electrochim Acta 2015;177:137–44.
[125] Zhang K, Gong S, Zhao B, Liu Y, Qaisrani NA, Li L, Zhang F, He G. Bent-twisted block copolymer anion exchange membrane with improved conductivity. J Membr Sci 2018;550:59–71.
[126] Wang C, Tao Z, Zhao X, Li J, Ren Q. Poly (aryl ether nitrile) s containing flexible side-chain-type quaternary phosphonium cations as anion exchange membranes. Sci China Mat 2020;63(4):533–43.
[127] Vijayakumar V, Nam SY. Recent advancements in applications of alkaline anion exchange membranes for polymer electrolyte fuel cells. J Ind Eng Chem 2019;70:70–86.
[128] Xu F, Su Y, Lin B. Progress of alkaline anion exchange membranes for fuel cells: the effects of micro-phase separation. Front Mat 2020;7(4).
[129] You W, Noonan KJT, Coates GW. Alkaline-stable anion exchange membranes: a review of synthetic approaches. Prog Polym Sci 2020;100:101177.
[130] Wang L, Peng X, Mustain WE, Varcoe JR. Radiation-grafted anion-exchange membranes: the switch from low-to high-density polyethylene leads to remarkably enhanced fuel cell performance. Energy Environ Sci 2019;12(5):1575–9.
[131] Shin DW, Guiver MD, Lee YM. Hydrocarbon-based polymer electrolyte membranes: importance of morphology on ion transport and membrane stability. Chem Rev 2017;117(6):4759–805.
[132] Zhang Z, Wu L, Varcoe J, Li C, Ong AL, Poynton S, Xu T. Aromatic polyelectrolytes via polyacylation of pre-quaternized monomers for alkaline fuel cells. J Mater Chem A 2013;1(7):2595–601.
[133] Kobayashi S, Müllen K. Encyclopedia of polymeric nanomaterials. Springer Berlin Heidelberg; 2015.
[134] Miller HA, Pagliaro MV, Bellini M, Bartoli F, Wang L, Salam I, Varcoe JR, Vizza F. Integration of a Pd-$CeO_2$/C anode with Pt and Pt-free cathode catalysts in high power density anion exchange membrane fuel cells. ACS Appl Energy Mater 2020;3(10):10209–14.
[135] Britton B, Holdcroft S. The control and effect of pore size distribution in AEMFC catalyst layers. J Electrochem Soc 2016;163(5):F353.
[136] Wang L, Bellini M, Miller HA, Varcoe JR. A high conductivity ultrathin anion-exchange membrane with 500+ h alkali stability for use in alkaline membrane fuel cells that can achieve 2 W $cm^{-2}$ at 80°C. J Mater Chem A 2018;6(31):15404–12.
[137] Xie L, Kirk DW. Platinum stability at the cathode of an anion exchange membrane fuel cell. Electrocatalysis 2020;11(3):292–300.
[138] P Leonard D, Maurya S, Park EJ, Manriquez LD, Noh S, Wang X, Bae C, Baca ED, Fujimoto C, Kim YS. Asymmetric electrode ionomer for low relative humidity operation of anion exchange membrane fuel cells. J Mater Chem A 2020;8(28):14135–44.
[139] Li D, Chung HT, Maurya S, Matanovic I, Kim YS. Impact of ionomer adsorption on alkaline hydrogen oxidation activity and fuel cell performance. Curr Opin Electrochem 2018;12:189–95.
[140] Park EJ, Maurya S, Lee AS, Leonard DP, Li D, Jeon JY, Bae C, Kim YS. How does a small structural change of anode ionomer make a big difference in alkaline membrane fuel cell performance? J Mater Chem A 2019;7(43):25040–6.
[141] Matanovic I, Maurya S, Park EJ, Jeon JY, Bae C, Kim YS. Adsorption of polyaromatic backbone impacts the performance of anion exchange membrane fuel cells. Chem Mater 2019;31(11):4195–204.
[142] Santori PG, Mondal AN, Dekel DR, Jaouen F. The critical importance of ionomers on the electrochemical activity of platinum and platinum-free catalysts for anion-exchange membrane fuel cells. Sustain Energy Fuels 2020;4(7):3300–7.
[143] Zhou T, He X, Lu Z. Studies on a novel anion-exchange membrane based on chitosan and ionized organic compounds with multiwalled carbon nanotubes for alkaline fuel cells. J Appl Polym Sci 2018;135(22):46323.